Summer 8-15-2018

Chemo-Thermo Cure of Viscoelastic Materials for Semiconductor Packaging Applications

Anjali Pradeep Kumar
Portland State University

Recommended Citation

Pradeep Kumar, Anjali, "Chemo-Thermo Cure of Viscoelastic Materials for Semiconductor Packaging Applications" (2018). *Dissertations and Theses.* Paper 4537.
https://doi.org/10.15760/etd.6422

Chemo-Thermo Cure of Viscoelastic Materials for Semiconductor Packaging Applicaitons

by

Anjali Pradeep Kumar

A thesis submitted in partial fulfillment of the
requirements for the degree of

Master of Science
in
Mechanical Engineering

Thesis Committee:
Sung Yi, Chair
Chien Wern
Faryar Etesami

Portland State University
2018

Abstract

Viscoelastic polymer materials are being actively considered as a novel material for semiconductor packaging applications as a result of their ability to develop strong adhesive bonds at lower temperatures. Viscoelastic thermoset materials are impacted by the stresses generated during the curing process, which is also accompanied by a dissipation of thermal energy. There is a need to develop a generic modeling formulation that is applicable to any material of interest in order to enable the study of different bonding materials and develop optimized curing cycles. This study reports a numerical formulation to evaluate the stress generated and energy dissipated during the cure of viscoelastic polymers. A generalized method to define the transient variation of degree of cure was developed using a 4^{th} order Runge Kutta approximation. The mathematical formulation was implemented using a novel evaluation methodology that helped reduce the computational power requirement. The commercially-available 3501-6 resin was simulated as a characteristic material in this study. The numerical model was validated against analytically derived solutions for both a single Maxwell model, and a Generalized Maxwell Model (GMM) for cases of constant-strain inputs, and subsequently for sinusoidal strain inputs, wherein, material properties were considered to be constant or varying linearly with degree of cure.

A good agreement was obtained between the present model and analytical solutions.

To my husband, Harish Ganapathy, and my family.

Acknowledgments

I would like to express my sincere gratitude to my graduate advisor, Professor Sung Yi, at Portland State University, for his mentorship during the past two years. He has been a constant source of encouragement, and has provided very valuable advice during difficult times in my research that has guided me towards making great progress. I am extremely thankful to have been given the opportunity to work under his guidance.

I would also like to thank all the faculty and staff of the Mechanical Engineering Department at Portland State University, who have been of great help during the course of my graduate studies.

Table of Contents

List of Figures

1 Introduction

Miniaturization of electronic devices and components has lead to several technological advances in a variety of fields such as consumer electronics, space technology, and defense systems, among others. Applications have been developed that require a need for higher computational power, packed on to smaller surface geometries, and the materials used in the construction of various IC packages are of great importance to their functionality and reliability (Tummala et al., 2002; Liu et al, 2008; Tu, 2011). Their mechanical, electrical, and chemical properties establish the foundation for electronic packaging, and ultimately its performance.

Epoxy resins are thermoset materials that are currently being used in several applications in semiconductor packaging due to their good mechanical and thermal properties. Epoxies are viscoelastic materials that are significantly influenced by the rate of straining or stressing. As the name implies, viscoelasticity combines both elastic and viscous properties and hence can be represented using various models that contain two main components, spring and dash-pot. Since time is a very important factor in their behavior, these materials can be characterized using constitutive equations that include time as a variable in addition to stress and strain. There are

of two types of viscoelastic polymers, linear viscoelastic materials and non-linear viscoelastic materials. Linear viscoelastic materials are those whose material properties remain constant, whereas, for non-linear viscoelastic polymers, properties vary with degree of cure. One of the most important characteristic of epoxy resins is their adhesion to numerous substances. Curing process can be described as a chemical reaction in which monomers cross-link to form a three-dimensional network resulting in a hard substance with excellent combination of mechanical, electrical, chemical and thermal properties. Adhesion strength of the polymer depends on the rate of curing, a more rapid cure results in a weaker bond. Hence, it is important to optimize the rate of curing.

Lee et al. (1982) experimentally determined the variation of material properties of viscoelastic polymer such as 3501-6 (amine-cured) epoxy resin system, which is used extensively in the industry. Empirical relations were developed for properties such as the heat of reaction, degree of cure, and viscosity as these influence the curing of the polymer. Results for heat of reaction and degree of cure were obtained by carrying out experiments using a Differential Scanning Calorimeter (DSC) under isothermal conditions for a range of temperatures as well at constant increasing rate and the relations obtained show how the degree of cure varies with time for a given temperature.

Loos and Springer (1983) reported models that simulated the curing of thermosetting materials by relating the curing process to the actual phenomena (chemical, thermal, physical) that are in occurrence within the composite. A computer code was developed, which accepted key inputs such as geometry, boundary conditions (temperature, pressure, initial cure state), material properties, etc., and was used to calculate the temperature distribution and resin flow in the composite. One of the applications of this effort was to enable the ability to determine an appropriate cure cycle for any given application with the broad objectives of minimizing cure time and maximizing cured-strength by reducing the occurrence of voids in the cured material.

Adolf and Martin (1996) reported a detailed theoretical analysis to determine the changes in material properties of a non-linear viscoelastic polymer as it undergoes curing, which involves cross-linking reactions, and is an exothermic process. Combining experimental data with their analysis, a power-law based correlation was proposed for the variation of shear modulus with degree of cure. The authors remarked on the specific applicability of their correlations for future modeling codes.

Yi and Hilton (1995) formulated, for the first time, cure-dependent mechanical response of thermosetting resins using models that represented their chemo-rheological behavior during the manufacturing process. These

polymers were modeled as viscoelastic models that had material properties that were dependent on time, temperature and cure-dependent parameters. The residual stresses and strain fields in the resin were calculated using these parameters for the entire time temperature history of the polymer during its curing process. Hilton and Yi (1992) also formulated expressions for stored and dissipation energies in a viscoelastic polymer in response to a given loading. These were also derived using generalized Maxwell models with varying material properties. Knowing the dissipation energy or the residual stresses, can help to chose a polymer for a specific purpose without carrying out detailed experimental analysis. Yi et al. (1997) also developed a finite element model to simulate the curing process in polymers to predict the temperature distributions throughout cure cycle. Polymers used for this study were Glass-polyster and Hercules AS4/3501-6 epoxy and these had non-linear viscoelastic characteristics wherein, their material properties were dependent on temperature and degree of cure. Temperature distributions from finite element analysis were compared with experimental results and a good agreement was obtained.

Polymers are used widely in electronic packaging applications. Once such application is their use as underfill in flip-chip packaging, to reduce relative movement between silicon chip and organic substrate caused by mismatch in coefficient of thermal expansion. Yi and Chian (2001), stud-

ied the importance of curing method in thermosetting polymers that are used as underfill for semiconductor applications. The chemical and thermal changes that occur to the polymer during cure was studied and empirical relations were developed to show the dependence of material properties on temperature and degree of cure. These correlations were obtained by modeling using time dependent standard viscoelastic models and determining the changes in their behavior while varying parameters such as temperature and degree of cure.

Yi et al. (2001) also investigated microwave curing process for undefill in flip chip packaging. This was used as an alternative to traditional thermal curing that takes a long time due to poor conductivity of the polymer wherein energy transfer takes place through conduction, convection or radiation from the surfaces. In microwave curing, energy is transferred through molecular interaction and therefore results in faster heating. The study was conducted using 3D finite element simulations for a variable frequency microwave and was verified using analytical calculations for simple conditions. Liu et al. (2004, 2005) also conducted further studies on microwave cure of underfill using finite element studies. Results from numerical analysis were obtained for various step sizes, and it was observed that a small change in step size can cause huge differences when compared to analytical solution. Cure kinetics of the underfill material was investigated for both microwave

and thermal curing using DSC, and no difference was found in reaction mechanism.

Yim and Paik (1998, 2006) provided a detailed study on the applications of Anisotropic Conductive Films (ACF). These are composed of adhesive epoxies with conductive fillers embedded and are used for LCD packaging technologies wherein the bonding can have fine pitch interconnect capability. This technology is an alternative to soldering due to higher connection resistance, lower bonding temperature that reduces residual stresses and fine pitch conduction pads as compared to solder bumps. They highlighted the advances in developing low temperature curable ACFs, which are particularly of interest for both LCD modules, as well as other semiconductor applications sensitive to the typical higher levels of bonding temperature. Several patents were filed by these authors including Yim and Paik (2001), Paik and Yim (2005).

Eom et al. (2000) developed two models to predict the change in viscoelastic properties of a thermoset resin by varying parameters such as time, temperature and degree of cure. This can be used to determine the internal stresses induced in the specimen when it undergoes processing. An amine-based epoxy resin was used to develop a cure kinetics model to obtain a relationship between time, temperature and degree of cure using a Differential scanning calorimeter and a phenomenological model to evaluate the

variation in relaxation modulus during the entire range of curing process.

Liang and Chandrashekhara (2006) reported an experimental study on the cure kinetics and rheological properties of a novel soy-based epoxy resin using DSC and viscometry, respectively. A neural network-based rheological model was proposed. This material was of particular interest due to its higher reactivity and therefore greater potential for cross-linking.

Yang et al. (2007) summarized the effect of polymer cure on the viscoelastic characteristics of polymers, and noted that the presence of filler materials has an opposite effect on residual stresses, because, with an increase in filler concentration, the glass and rubbery modulus increases, while the coefficients of thermal expansion and cure-caused shrinkage decreases. Accordingly, they investigated the suitability of models to accurately model the effect of filler concentration on shear/bulk moduli and coefficient of thermal expansion. Novolac Bisphenol-A compound was used in this study and it was found that Eilers model was most applicable for the variation of fully cured shear modulus with filler concentration, and a differential scheme method was better suited for describing the bulk modulus.

Zhang et al. (2009) developed a 3-D FEM model to predict the temperature and degree of cure of an epoxy undergoing cure, and this model was subsequently used to study the effect of different cure ramp cycles on the degree of cure. The data predicted by the model was successfully validated

against experimental data.

Sadeghinia et al. (2012a) studied the changes in the viscoelastic properties of an epoxy adhesive compound, Novolac Bisphenol-A. Differential scanning calorimetry (DSC) and high-pressure dilatometry was used to measure the cure kinetics, coefficient of thermal expansion, and shrinkage during cure. The storage modulus, which is dependent on time and temperature, was measured using a Dynamic Mechanical Analyzer (DMA). The effect of filler on these properties was also investigated. It was reported that the presence of filler reduced the shrinkage of epoxy during cure. Their study fitted the experimentally obtained data to regression-based models. Subsequently, Sadeghinia et al. (2012b) investigated the change in viscoelastic properties of the same epoxy compound during the curing process with a DMA. They conducted an intermittent cure test that collected transient data to derive the shear modulus. DSC was used to drive the change in glass transition temperature with respect to the degree of cure. Their data for cure-dependent shear modulus was compared against the scaling law of Adolf and Martin (1996) and a good agreement was reported.

Hossain et al. (2009, 2014), reported a detailed review of models for viscoelastic cure of polymers. They reported a cure-dependent thermodynamically consistent model to simulate small strain deformations. Saseendran et al. (2016) reported two experimental approaches that exposed the LY5052

epoxy resin system to various curing temperature/time sequences and analyzed the viscoelastic properties using Dynamic Mechanical and Thermal Analysis (DMTA) equipment, that yielded a greater understanding of these properties in the glassy and rubbery regions. Carlone et al. (2014) highlighted the necessity of simulation models to aid in the optimization of cure cycles, and proposed an artificial neural network (ANN)-based meta-model for this purpose which involved coupling an FEM thermo-chemical model of the curing process with ANN.

The above brief literature review indicates relatively few studies have focused on modeling the stress-strain characteristics of viscoelastic polymer materials in a form that is generalized and applicable to any other material as well. There is a need to develop a generic modeling formulation that is not heavily reliant on empirical data and thereby limited to only those bonding materials, but rather uses fundamental equations to model the curing process. In this thesis, a numerical formulation has been reported to evaluate the stresses generated during the chemo-thermo cure of viscoelastic polymer materials. The viscoelastic material was modeled using the Maxwell model. The variation of degree of cure with time is a key input to this formulation, and the 4^{th} order Runge Kutta-based method was used in order to define this relationship, and thereby enabling its generic applicability to any polymer material. Subsequently, the predicted stress was used to

determine the energy dissipated during the curing process. Since this process is transient in nature, an effort was made to reduce the computational requirements which are directly proportional to the duration of time that is being simulated. Accordingly, a novel modeling methodology was developed, wherein, key functional terms are evaluated only once and stored for subsequent usage in the evaluation of stress. As a test case, the commercially available 3501-6 resin was simulated on account of its well-reported reaction kinetics and rate of cure characteristics in the literature. For this test case, the modeling methodology included determination of the change in temperature based on disspation energy, and subsequently used the new temperature value for stress calculations at subsequent time intervals. For validation purposes, the numerical model was compared against an analytically derived solution for a constant strain input, and a good agreement was obtained. Finally, this formulation was extended for the case of a Generalized Maxwell Model (GMM). The results from GMM case were also compared against an analytical derived solution and a good agreement was obtained.

2 Cure Reaction Kinetics

2.1 Differential scanning calorimetry

The cure kinetics model for a polymer can be used to predict the degree of cure and reaction rate which vary with time and temperature. This can be experimentally obtained based on the data obtained using Differential Scanning Calorimetry (DSC). DSC is a thermal analysis technique which is used to measure the heat flow rate required to increase the temperature of a sample and a reference, as a function of time. The underlying principle is that, as the sample undergoes a phase change, it results in an exothermic or endothermic reaction based on the amount of heat that flows into the sample to maintain itself and the reference sample at the same temperature. DSC measures the heat of reaction and thereby the degree of cure for an epoxy resin over a wide range of temperatures.

Two different methods are used to examine the cure kinetics of a polymer: Isothermal Scanning - where the sample is maintained at constant temperature, and Dynamic Scanning - wherein the sample is heated at a constant rate over a given range of temperatures. In dynamic measurements, the rate of heat generated, (dQ), is plotted against time, and area under the curve is used to determine the heat of reaction which is given by

Eq.(2.1) wherein, H_R refers to the total heat of the reaction and t_f is the total time taken for the reaction to be completed.

$$H_R = \int_0^{t_f} \frac{dQ}{dt} dt \tag{2.1}$$

Isothermal measurements are used to determine the amount of heat released until a given time t, by plotting the rate of heat generated (dQ) versus time and integrating the area of the exothermic peak given by Eq.(2.2) wherein H refers to the heat of reaction up to time t.

$$H = \int_0^{t} \frac{dQ}{dt} dt \tag{2.2}$$

The value for degree of cure α of any given polymer ranges from 0 (being completely uncured) to 1 (fully cured) and can be obtained as

$$\alpha(t) = \frac{H}{H_R} \tag{2.3}$$

Then, the rate of degree of cure is calculated as

$$\frac{d\alpha}{dt} = \frac{dQ}{dt} \frac{1}{H_R} \tag{2.4}$$

2.2 Generalized model to calculate degree of cure

Various cure kinetic models have been developed in order to describe the curing process of thermoset resins. Among these, nth order and bi-nodal models are widely used for the modeling of thermosetting polymers. The

nth order kinetics can be expressed as

$$\frac{d\alpha}{dt} = k_0(1-\alpha)^n \tag{2.5}$$

Another model proposed by Kamal et al. is as shown below

$$\frac{d\alpha}{dt} = (k_1 + k_2\alpha^m)(1-\alpha)^n \tag{2.6}$$

In the equations above, k_0, k_1 and k_2 are rate constants, which depend on temperature, material properties, and m and n are constants. The above equations can be solved for any given value of m and n by using an efficient numerical method to evaluate first order ordinary differential equations. In this study, the Runge Kutta 4^{th} order method has been used to solve the ordinary differential equations as given in Eq.(2.5) and (2.6) to obtain a relation between degree of cure, α, and time, t. Let us define the rate of cure as

$$\frac{d\alpha}{dt} = f(t,\alpha) \tag{2.7}$$

The curing process starts at time, t_0, increments in steps of dt , and proceeds until the final time t_f. Then step size, h, is given by, $h = dt/N$. Accuracy of the numerical model can be increased by using a smaller value for h. In order to solve the ordinary differential equation in Eq.(2.7), an initial condition for degree of cure (α) is required.

$$\alpha(t = t_0) = y_0 \tag{2.8}$$

Let B_1 be the slope at the beginning of the time step (t_0).

$$B_1 = f(t_0, y_0) \tag{2.9}$$

If we use the slope B_1 to step halfway through the time step, then B_2 is an estimate of the slope at the midpoint.

$$B_2 = f(t_0 + \frac{h}{2}, y_0 + \frac{B_1}{2}h) \tag{2.10}$$

If we use the slope B_2 to step halfway through the time step, then B_3 is another estimate of the slope at the midpoint.

$$B_3 = f(t_0 + \frac{h}{2}, y_0 + \frac{B_2}{2}h) \tag{2.11}$$

Finally, B_4 is an estimate of the slope at the end point.

$$B_4 = f(t_0 + h, y_0 + hB_3) \tag{2.12}$$

We then use a weighted sum of these sloped to get the final estimate of $t_1 = t_0 + h$ as,

$$y_1 = y_0 + \frac{h}{6}(B_1 + 2B_2 + 2B_3 + B_4) \tag{2.13}$$

Numerical model validation

Lee et al. (1982) conducted an experimental investigation of the key properties of a commercially available resin 3501-6 and reported correlations that

relate the rate of cure with reaction kinetics. By using Dynamic Scanning Calorimetry (DSC), it was identified that heat generated during the curing process has two peaks (refer to Figure 2.1) as a result of separate reactions that occur during the curing process, with the shift occurring at a degree of cure of 0.3. Accordingly, two separate correlations were developed for cures below and above this threshold value as

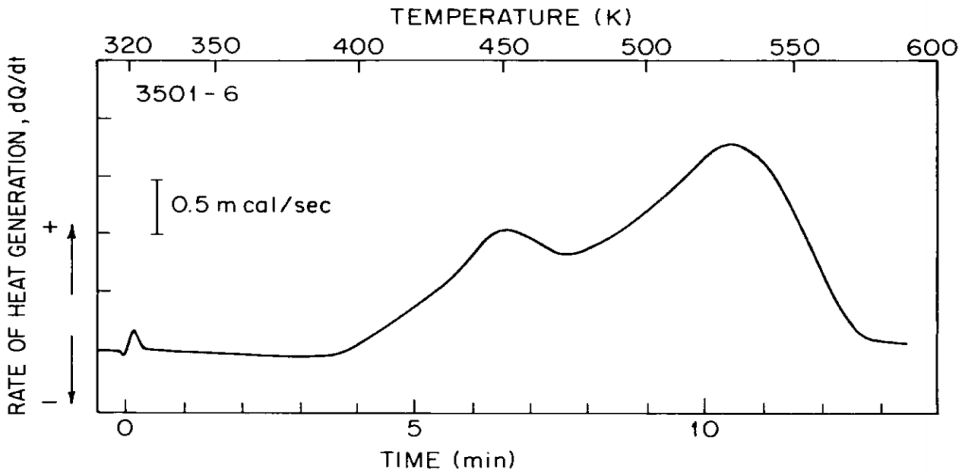

Figure 2.1: Rate of heat generation versus time for resin 3501-6 (Lee et al., 1980)

For $\alpha \leq 0.3$

$$\frac{d\alpha}{dt} = (K_1 + K_2\alpha)(1-\alpha)(B-\alpha) \tag{2.14}$$

For $\alpha > 0.3$

$$\frac{d\alpha}{dt} = K_3(1-\alpha) \tag{2.15}$$

where

$$K_1 = A_1 \exp(-\triangle E_1/RT) \tag{2.16}$$

$$K_2 = A_2 \exp(-\triangle E_2/RT) \tag{2.17}$$

$$K_3 = A_3 \exp(-\triangle E_3/RT) \tag{2.18}$$

A_1, A_2 and A_3 are pre-exponential factors given by

$$A_1 = 2.101 \times 10^9 \ min^{-1}$$

$$A_2 = -2.014 \times 10^9 \ min^{-1}$$

$$A_3 = 1.960 \times 10^9 \ min^{-1}$$

$\triangle E_1$, $\triangle E_2$ and $\triangle E_3$ are activation energies given by

$$\triangle E_1 = 8.07 \times 10^4 \ J/mol$$

$$\triangle E_2 = 778 \times 10^4 \ J/mol$$

$$\triangle E_3 = 5.66 \times 10^4 \ J/mol$$

R is the universal gas constant given by 8.314 $J/molK$, B is constant with a value of 0.47 ± 0.07.

In order to validate the numerical model, Eqs.(2.14) and (2.15) have been solved analytically and the results are compared with the numerical solution. Once the results are verified for this simple viscoelastic model, the same numerical analysis can be used to determine cure kinetic relations for any composite polymer. Analytical solution for rate of change of degree of cure relation with respect to time is given below.

Solving for Eq.(2.14) for $\alpha \leq 0.3$ lead to

$$\frac{d\alpha}{(K_1 + K_2\alpha)(1-\alpha)(B-\alpha)} = dt \tag{2.19}$$

$$\frac{d\alpha}{K_2(\frac{K_1}{K_2} + \alpha)(\alpha-1)(\alpha-B)} = dt \tag{2.20}$$

$$\frac{d\alpha}{(k+\alpha)(\alpha-1)(\alpha-B)} = K_2 dt \tag{2.21}$$

where $k = K_1/K_2$.

Separately evaluating L.H.S of Eq.(2.21) as

$$\frac{1}{(k+\alpha)(\alpha-1)(\alpha-B)} = \frac{a}{\alpha-1} + \frac{b}{\alpha-B} + \frac{c}{(k+\alpha)} \tag{2.22}$$

$$= \frac{1}{g(\alpha)}[a(\alpha-S)(\alpha+k) + b(\alpha-1)(\alpha+k) + c(\alpha-1)(\alpha-S)]$$

$$= \frac{1}{g(\alpha)}[a(\alpha^2-(B-k)\alpha-Bk)+b(\alpha^2-(1-k)\alpha-k)+c(\alpha^2-(1+B)\alpha+B)]$$

$$= \frac{1}{g(\alpha)}[(a+b+c)\alpha^2-\{a(B-k)+b(1-k)+c(1+B)\}\alpha-aBk-bk+cB]$$

where

$$g(\alpha) = (\alpha-1)(\alpha-B)(\alpha+k) \tag{2.23}$$

Constants a, b and c should be chosen such that the numerators for L.H.S and R.H.S in Eq.(2.22) are equal for every α.

$$a + b + c = 0 \tag{2.24}$$

$$-a(B-k) - b(1-k) - c(1+B) = 0 \tag{2.25}$$

$$-aBk - bk + cB = 1 \tag{2.26}$$

We can rewrite the above equations in matrix form as

$$Gx = y \tag{2.27}$$

where

$$G = \begin{bmatrix} 1 & 1 & 1 \\ -(B-k) & -(1-k) & -(1+B) \\ -Bk & -k & B \end{bmatrix} \tag{2.28}$$

$$x = \begin{pmatrix} a \\ b \\ c \end{pmatrix} \tag{2.29}$$

and

$$y = \begin{pmatrix} 0 \\ 0 \\ 1 \end{pmatrix} \tag{2.30}$$

We can solve the above equation by taking the inverse of G such that $x = G^{-1}y$ where,

$$G^{-1} = \frac{1}{|G|} \begin{bmatrix} -B-1 & -B-1 & -B-1 \\ B^2(1+k) & B(1+k) & (1+k) \\ -k^2(1-B) & k(1-B) & -(1-B) \end{bmatrix} \tag{2.31}$$

wherein determinant of G is given as

$$|G| = -B - B^2 - k + B^2k - k^2 + Bk^2 \tag{2.32}$$

$$= (k+1)B^2 + (k^2-1)B - (k^2+k) \tag{2.33}$$

Accordingly, we obtain

$$x = \begin{pmatrix} a \\ b \\ c \end{pmatrix} = \frac{1}{|G|} \begin{pmatrix} -B-k \\ 1+k \\ -1+B \end{pmatrix} \tag{2.34}$$

Eq.(2.21) can be re-written as

$$\frac{a\ d\alpha}{\alpha - 1} + \frac{b\ d\alpha}{\alpha - B} + \frac{c\ d\alpha}{(\alpha + k)} = K_2 dt \tag{2.35}$$

$$-\frac{a\ d\alpha}{1-\alpha} - \frac{b\ d\alpha}{B-\alpha} + \frac{c\ d\alpha}{(k+\alpha)} = K_2 dt \tag{2.36}$$

$$-\frac{a\ d\alpha}{1-\alpha} - \frac{b\ d\alpha}{B(1-\frac{\alpha}{B})} + \frac{c\ d\alpha}{k(1-\frac{\alpha}{k})} = K_2 dt \tag{2.37}$$

Integrating Eq.(2.37) leads to

$$-a(-1)\ \ln|1-\alpha| - \frac{b}{B}(-B)\ \ln|1-\frac{\alpha}{B}| + \frac{c}{k}(k)\ \ln|1+\frac{\alpha}{k}| = K_2 t + const \tag{2.38}$$

$$a\ \ln|1-\alpha| + b\ \ln|1-\frac{\alpha}{B}| + c\ \ln|1+\frac{\alpha}{k}| = K_2 t + const \tag{2.39}$$

At $t = 0$, $\alpha = 0$, therefore, $const = 0$. Then we have

$$a\ \ln|1-\alpha| + b\ \ln|1-\frac{\alpha}{B}| + c\ \ln|1+\frac{\alpha}{k}| = K_2 t \tag{2.40}$$

Finally,

$$t = \left(\frac{a}{K_2}\right)\ \ln|1-\alpha| + \left(\frac{b}{K_2}\right)\ \ln|1-\frac{\alpha}{B}| + \left(\frac{c}{K_2}\right)\ \ln|1+\frac{\alpha}{k}| \tag{2.41}$$

where

$$a = \frac{-B-k}{(k+1)B^2+(k^2-1)B-(k^2+k)}$$

$$= \frac{-B-\frac{K_1}{K_2}}{(\frac{K_1}{K_2}+1)B^2+((\frac{K_1}{K_2})^2-1)B-((\frac{K_1}{K_2})^2+k)}$$

$$= \frac{-(K_2B+K_1)K_2}{(K_1K_2+{K_2}^2)B^2+({K_1}^2-{K_2}^2)B-({K_1}^2+K_1K_2)}$$

$$= \frac{-(K_2B+K_1)K_2}{(K_1+K_2)(K_2B^2+(K_1-K_2)B-K_1)}$$

$$= \frac{-(K_2B+K_1)K_2}{(K_1+K_2)(K_2B+K_1)(B+1)} = \frac{-K_2}{(K_1+K_2)(B-1)} \tag{2.42}$$

$$b = \frac{1+k}{(k+1)B^2+(k^2-1)B-(k^2+k)}$$

$$= \frac{1+k}{(\frac{K_1}{K_2}+1)B^2+((\frac{K_1}{K_2})^2-1)B-((\frac{K_1}{K_2})^2+k)}$$

$$= \frac{(K_2+K_1)K_2}{(K_1K_2+{K_2}^2)B^2+({K_1}^2-{K_2}^2)B-({K_1}^2+K_1K_2)}$$

$$= \frac{(K_2+K_1)K_2}{(K_1+K_2)(K_2B+K_1)(B-1)} = \frac{K_2}{(K_2B+K_1)(B-1)} \tag{2.43}$$

$$c = \frac{-1+B}{(k+1)B^2+(k^2-1)B-(k^2+k)}$$

$$= \frac{-1+B}{(\frac{K_1}{K_2}+1)B^2+((\frac{K_1}{K_2})^2-1)B-((\frac{K_1}{K_2})^2+k)}$$

$$= \frac{(B-1){K_2}^2}{(K_1K_2+{K_2}^2)B^2+({K_1}^2-{K_2}^2)B-({K_1}^2+K_1K_2)}$$

$$= \frac{(B-1){K_2}^2}{(K_1+K_2)(K_2B+K_1)(B-1)} = \frac{{K_2}^2}{(K_1+K_2)(K_2B+K_1)} \tag{2.44}$$

Therefore,

$$\frac{a}{K_2} = \frac{-1}{(K_1+K_2)(B-1)} \tag{2.45}$$

$$\frac{b}{K_2} = \frac{1}{(K_2B+K_1)(B-1)} \tag{2.46}$$

$$\frac{c}{K_2} = \frac{K_2}{(K_1+K_2)(K_2B+K_1)} \tag{2.47}$$

Substituting the above equations into Eq.(2.41) leads to

$$t = \frac{-1}{(K_1+K_2)(B-1)}\ \ln|1-\alpha| + \frac{1}{(K_2B+K_1)(B-1)}\ \ln|1-\frac{\alpha}{B}|$$

$$+\frac{K_2}{(K_1+K_2)(K_2B+K_1)}\ \ln|1+\frac{K_2\alpha}{K_1}| \tag{2.48}$$

Analytical solution for the rate of change of degree of cure Eq.(2.15) for $\alpha > 0.3$ is given by

$$\frac{d\alpha}{dt} = K_3(1-\alpha) \tag{2.49}$$

Re-arranging the above equation and integrating yields,

$$\int \frac{d\alpha}{(1-\alpha)} = \int K_3 dt + C \tag{2.50}$$

$$-\ln(1-\alpha) = K_3 t + C \tag{2.51}$$

The initial condition used to solve Eq.(2.51) is

At $\alpha = 0.3$, $t = t_c$ where t_c is obtained by substituting $\alpha = 0.3$ into Eq.(2.48),

$$t_c = \frac{-1}{(K_1+K_2)(B-1)}\ln(0.7) + \frac{1}{(K_2B+K_1)(B-1)}\ln|1-\frac{0.3}{B}|$$

$$+\frac{K_2}{(K_1+K_2)(K_2B+K_1)}\ln|1+\frac{0.3K_2}{K_1}| \tag{2.52}$$

Then Eq.(2.51) becomes

$$-\ln(1-\alpha) = K_3 t - \ln(0.7) - K_3 t_c \tag{2.53}$$

Therefore, for $\alpha > 0.3$, we have

$$t = -\frac{1}{K_3}\ln\frac{(1-\alpha)}{0.7} + t_c \tag{2.54}$$

Eqs.(2.14) and (2.15) have been modeled numerically using the Runge Kutta 4^{th} order numerical method. Let us define

$$y = \frac{d\alpha}{dt} = f(\alpha(t), t) \tag{2.55}$$

For $\alpha \leq 0.3$, initial conditions are, $\alpha = 0$, $t = 0$ and f is

$$f(\alpha(t), t) = (K_1 + K_2\alpha)(1 - \alpha)(B - \alpha) \tag{2.56}$$

For $\alpha > 0.3$, initial conditions are, $\alpha = 0.3$, $t = t_c$ and f is

$$f(\alpha(t), t) = K_3(1 - \alpha) \tag{2.57}$$

This numerical method has been used to approximate the value of α by numerically solving the first order ordinary differential Eqs.(2.56) and (2.57) using a step size h that is used to approximate the degree of cure. Fig. 2.2 is a plot of degree of cure α vs. time from $t = 0$ to $t = 200s$ in steps of $dt = 0.1s$ for a temperature of 450K and time step $h = dt/5$. This can be used to calculate the four weighted averages as

$$B_1 = f(t_0, y_0) \tag{2.58}$$

where B_1 is the slope $f(t, \alpha)$ at the beginning of the time step $t = t_0$.

$$B_2 = f(t_p + \frac{h}{2}, y_p + \frac{B_1}{2}h) \tag{2.59}$$

B_2 is the estimate of the slope at $t = t_0 + h/2$

$$B_3 = f(t_p + \frac{h}{2}, y_p + \frac{B_2}{2}h) \tag{2.60}$$

B_3 is another estimate of the slope at $t = t_0 + h/2$

$$B_4 = f(t_p + h, y_p + hB_3) \tag{2.61}$$

B_4 is the estimate of the slope at $t = t_0 + h$

Then y becomes

$$y(t_0 + h) = y(t_0) + \frac{h}{6}(B_1 + 2B_2 + 2B_3 + B_4) \tag{2.62}$$

The analytical and numerical solutions for Eqs.(2.14) and (2.15) have been combined in Fig. 2.2. It was observed that the accuracy of the plot does not change by reducing time interval or increasing the step size for the numerical model.

The variation of degree of cure, α, with respect to time for various temperatures have also been plotted in Fig.2.3. It can be observed that polymer cures at shorter intervals of time at higher temperature.

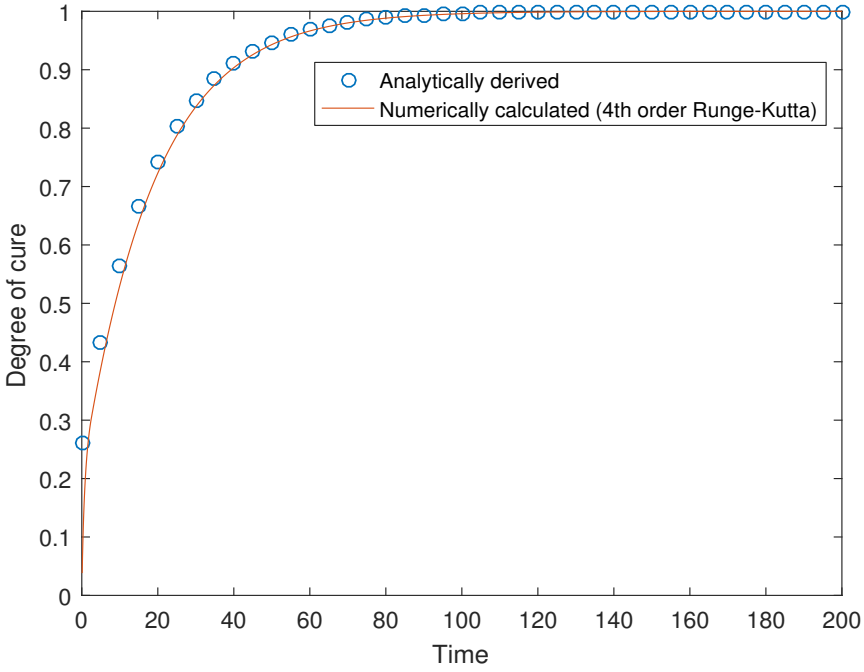

Figure 2.2: Degree of cure vs Time (for a Temp=450K).

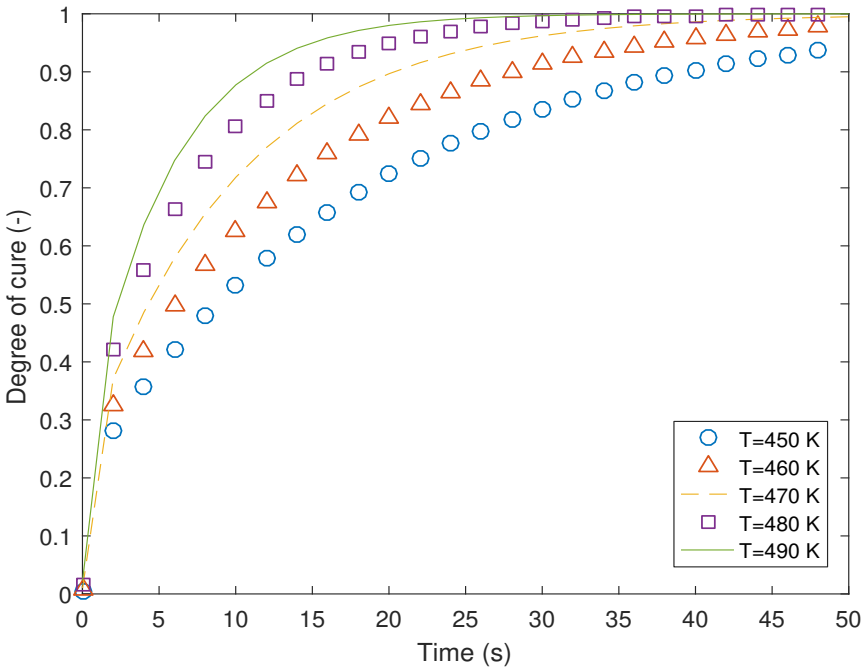

Figure 2.3: Degree of cure vs Time for various temperatures.

3 Modeling Methodology

3.1 Introduction to Maxwell Model

Consider a viscoelastic polymer represented as a single Maxwell model as shown in Fig.(3.1) that has time and temperature dependent material properties $G(t,T)$ and $\eta(t,T)$.

Figure 3.1: Schematic of a Maxwell model.

The stress-strain relation for spring and dashpot are as follows

$$\gamma_{kl}^{(G)}(x,t) = \frac{\tau_{kl}(x,t)}{2G(t,T)} \tag{3.1}$$

$$\frac{\partial \gamma_{kl}^{(\eta)}(x,t)}{\partial t} = \frac{\tau_{kl}(x,t)}{2\eta(t,T)} \tag{3.2}$$

$$\tau_{kl} = \tau_{kl}^{(G)} = \tau_{kl}^{(\eta)} \tag{3.3}$$

$$\gamma_{kl} = \gamma_{kl}^{(G)} + \gamma_{kl}^{(\eta)} \tag{3.4}$$

where τ_{kl} is the total stresses in the model which is the same in the spring and dashpot, γ_{kl} is the total strain which is the sum of individual strains of spring and dashpot when connected in series.

Differentiating Eq.(3.4) yields

$$\frac{d\gamma_{kl}}{dt} = \frac{d\gamma_{kl}^{(G)}}{dt} + \frac{d\gamma_{kl}^{(\eta)}}{dt} \tag{3.5}$$

Substituting Eq.(3.1) and Eq.(3.2) into Eq.(3.5) leads to

$$\frac{\partial \gamma_{kl}(x,t)}{\partial t} = \frac{\partial}{\partial t}\left(\frac{\tau_{kl}(x,t)}{2G(t,T)}\right) + \frac{\tau_{kl}(x,t)}{2\eta(t,T)}$$

$$= \frac{1}{2G(t,T)}\frac{\partial}{\partial t}\left(\tau_{kl}(x,t)\right) + \tau_{kl}(x,t)\frac{\partial}{\partial t}\left(\frac{1}{2G(t,T)}\right) + \frac{\tau_{kl}(x,t)}{2\eta(t,T)} \tag{3.6}$$

Multiplying Eq.(3.6) by $2G(t,T)$ yields

$$2G(t,T)\frac{\partial \gamma_{kl}(x,t)}{\partial t} = \frac{\partial \tau_{kl}(x,t)}{\partial t} + \tau_{kl}\left[G(t,T)\frac{\partial}{\partial t}\left(\frac{1}{G(t,T)}\right) + \frac{G(t,T)}{\eta(t,T)}\right] \tag{3.7}$$

Rearranging Eq.(3.7) we obtain

$$\frac{\partial \tau_{kl}(x,t)}{\partial t} + \frac{\tau_{kl}(x,t)}{\lambda(t,T)} = 2G(t,T)\frac{\partial \gamma_{kl}(x,t)}{\partial t} \tag{3.8}$$

where λ is the relaxation time defined as

$$\frac{1}{\lambda(t,T)} = \left[G(t,T)\frac{\partial}{\partial t}\left(\frac{1}{G(t,T)}\right) + \frac{G(t,T)}{\eta(t,T)}\right] \tag{3.9}$$

Eq.(3.8) is a linear, non-homogeneous first order ODE of the form $\dot{x} + p(t)x = q(t)$ which has an analytic solution

$$x = \frac{1}{u(t)} \left(\int u(t)q(t)dt + C \right)$$

where, $u(t) = e^{\int p(t)dt}$, $\quad p(t) = \frac{1}{\lambda(t)}, \quad q(t) = 2G\dot{\gamma}$

Therefore, solution for Eq.(3.8) is given as,

$$\tau_{kl}(x,t) = 2e^{-F(x,t)} \int_0^t e^{F(x,t')} G(T,t,t') \frac{\partial \gamma_{kl}(x,t')}{\partial t'} dt' + Ce^{-F(x,t)} \tag{3.10}$$

where,

$$F(x,t) = \int_0^t \frac{dt}{\lambda(x,t,T)} = \int_0^t \left[G(t,T) \frac{\partial}{\partial t} \left(\frac{1}{G(t,T)} \right) + \frac{G(t,T)}{\eta(t,T)} \right] dt \tag{3.11}$$

The constant C in Eq.(3.10) can be obtained using initial condition

$$\gamma_{kl}(x,0) = \gamma_{kl}^{(G)}(x,0) = \frac{\tau_{kl}(x,0)}{2G(0,T)}$$

Therefore,

$$\tau_{kl}(x,0) = 2G(0,T)\gamma_{kl}(x,0) \tag{3.12}$$

Evaluating C by substituting Eq.(3.12) into Eq.(3.10) for time, $t = 0$.

$$C = \tau_{kl}(x,0)e^{F(x,0)} = 2G(0,T)\gamma_{kl}(x,0)e^{F(x,0)} \tag{3.13}$$

where

$$F(x,0) = \int_0^0 \left[G(t,T) \frac{\partial}{\partial t} \left(\frac{1}{G(t,T)} \right) + \frac{G(t,T)}{\eta(t,T)} \right] dt = 0 \tag{3.14}$$

Therefore,

$$e^{F(x,0)} = e^0 = 1 \tag{3.15}$$

Then,

$$C = \tau_{kl}(x,0)e^{F(x,0)} = 2G(0,T)\gamma_{kl}(x,0) \tag{3.16}$$

By substituting Eq.(3.16) into Eq.(3.10), the stress-strain relation for a single Maxwell model is given as

$$\tau_{kl}(x,t) = 2G(0,T)\gamma_{kl}(x,0)e^{-F(x,t)} + 2\int_0^t e^{-[F(x,t)-F(x,t')]}G(T,t,t')\frac{\partial\gamma_{kl}(x,t')}{\partial t'}dt' \tag{3.17}$$

In this study, the time dependent material co-efficients $G(t,T)$ and $\eta(t,T)$ are assumed to vary linearly with degree of cure and are, therefore, expressed as

$$G(\alpha(t,T)) = G_0 + G_1\alpha \tag{3.18}$$

$$\eta(\alpha(t,T)) = \eta_0 + \eta_1\alpha \tag{3.19}$$

Substituting Eqs.(3.18) and (3.19) into Eq.(3.11), $F(x,t)$ can be expressed as

$$F(x,t) = \int_0^t \frac{G_0 + G_1(\alpha)}{\eta_0 + \eta_1(\alpha)}dt \quad -\int_0^t \frac{\partial}{\partial t}[G_0+G_1(\alpha)]\left(\frac{1}{G_0 + G_1(\alpha)}\right)dt \tag{3.20}$$

3.2 Numerical analysis of stress-strain characteristics

Consider a viscoelastic polymer represented as a Maxwell model with strain input, $\gamma_{kl}(x,t)$, applied to the model until time, t_p. Then,

$$\tau_{kl}(x,t) = 2G(0,T)\gamma_{kl}(x,0)e^{-F(x,t_p)} + 2\int_0^{t_p} e^{-[F(x,t)-F(x,t')]}G(T,t,t')\frac{\partial\gamma_{kl}(x,t')}{\partial t'}dt' \tag{3.21}$$

The equation above can be solved numerically by discretization of the strain input $\gamma_{kl}(x,t)$ for very small time intervals such that $\triangle\gamma_{kl}(t_n)$ is constant over $\triangle t_n$, accordingly,

$$\begin{aligned}\tau_{kl}(x,t) &= 2G(0,T)\gamma_{kl}(x,0)e^{-F(x,t_p)} \\ &+ \quad 2\sum_{n=1}^{p}\int_{t_{n-1}}^{t_n} e^{-[F(x,t_p)-F(x,t')]}G(t,t',T)dt'\frac{\triangle\gamma_{kl}(t_n)}{\triangle t_n}\end{aligned} \tag{3.22}$$

Adding and subtracting $F(x,t_n)$ to $[F(x,t') - F(x,t_p)]$, Eq.(3.22) can be re-written as

$$\begin{aligned}\tau_{kl}(x,t) &= 2G(0,T)\gamma_{kl}(x,0)e^{-F(x,t_p)} \\ &+2\sum_{n=1}^{p}\int_{t_{n-1}}^{t_n} e^{[F(x,t')-F(x,t_p)+F(x,t_n)-F(x,t_n)]}G(t,t',T)dt'\frac{\triangle\gamma_{kl}(t_n)}{\triangle t_n}\end{aligned}$$

$$\begin{aligned}&= 2G(0,T)\gamma_{kl}(x,0)e^{-F(x,t_p)} \\ &+ \quad 2\sum_{n=1}^{p} e^{[F(x,t_n)-F(x,t_p)]}\int_{t_{n-1}}^{t_n} e^{[F(x,t')-F(x,t_n)]}G(t,t',T)dt'\frac{\triangle\gamma_{kl}(t_n)}{\triangle t_n}\end{aligned} \tag{3.23}$$

Eq.(3.23) can be re-written as

$$\tau_{kl}(x,t) = 2G(0,T)\gamma_{kl}(x,0)e^{-F(x,t_p)}$$

$$+ \quad 2\int_{t_{p-1}}^{t_p} e^{[F(x,t')-F(x,t_p)]}G(t,t',T)dt'\frac{\triangle\gamma_{kl}(t_p)}{\triangle t_p}$$

$$+ \quad 2\sum_{n=1}^{p-1} e^{[F(x,t_n)-F(x,t_p)]}\int_{t_{n-1}}^{t_n} e^{[F(x,t')-F(x,t_n)]}G(t,t',T)dt'\frac{\triangle\gamma_{kl}(t_n)}{\triangle t_n} \quad (3.24)$$

Let us define h as

$$h(t_p) = \frac{2}{\triangle t_p}\int_{t_{p-1}}^{t_p} e^{[F(x,t')-F(x,t_p)]}G(t,t',T)dt'$$

$$= \frac{2}{\triangle t_p}e^{-F(x,t_p)}\int_{t_{p-1}}^{t_p} e^{F(x,t')}G(t,t',T)dt' \quad (3.25)$$

The definite integral in Eq.(3.25) is evaluated using the Trapezoidal rule that works by approximating the region under the curve as a trapezoid which is obtained by plotting $f(t)$ with respect to time, t and calculating the area. Let,$f(t) = e^{F(x,t')}G(t,t',T)$, then

$$\int_{t_{p-1}}^{t_p} f(t)dt = \frac{(t_p - t_{p-1})}{2}\left[f(t_{(p-1)}) + f(t_{(p)})\right] \quad (3.26)$$

The results of the integral can be approximated by partitioning the integration interval (into N parts), applying the trapezoidal rule to each sub-interval, and summing the results. Then h becomes

$$h(t_p) = \frac{2}{\triangle t_p}e^{-F(x,t_p)}\sum_{n=1}^{p}\frac{(t_n - t_{n-1})}{2}\left[f(t_{(n-1)}) + f(t_{(n)})\right] \quad (3.27)$$

Then Eq.(3.24) becomes

$$\tau_{kl}(x,t) = \quad 2G(x,0)\gamma_{kl}(x,0)e^{-F(x,t_p)} \quad + \quad h(t_p)\triangle\gamma_{kl}(t_p)$$

$$+ \quad \sum_{n=1}^{p-1} e^{[F(x,t_n)-F(x,t_p)]} h(t_n) \triangle \gamma_{kl}(t_n) \tag{3.28}$$

Let us define R_p as

$$R_p = \sum_{n=1}^{p-1} e^{[F(x,t_n)-F(x,t_p)]} h(t_n) \triangle \gamma_{kl}(t_n) \tag{3.29}$$

Then we have

$$R_{p-1} = \sum_{n=1}^{p-2} e^{[F(x,t_n)-F(x,t_{p-1})]} h(t_n) \triangle \gamma_{kl}(t_n) \tag{3.30}$$

Then R_p can be re-written as

$$\begin{aligned} R_p &= e^{[F(x,t_{p-1})-F(x,t_p)]} h(t_{p-1}) \triangle \gamma_{kl}(t_{p-1}) \\ &+ \quad \sum_{n=1}^{p-2} e^{[F(x,t_n)-F(x,t_p)]} h(t_n) \triangle \gamma_{kl}(t_n) \end{aligned} \tag{3.31}$$

$$\begin{aligned} &= \quad e^{[F(x,t_{p-1})-F(x,t_p)]} h(t_{p-1}) \triangle \gamma_{kl}(t_{p-1}) \\ &+ \quad e^{[F(x,t_{p-1})-F(x,t_p)]} \sum_{n=1}^{p-2} e^{[F(x,t_n)-F(x,t_{p-1})]} h(t_n) \triangle \gamma_{kl}(t_n) \end{aligned}$$

Therefore,

$$R_p = e^{[F(x,t_{p-1})-F(x,t_p)]} \left[h(t_{p-1}) \triangle \gamma_{kl}(t_{p-1}) + R_{p-1} \right] \tag{3.32}$$

Then,

$$\tau_{kl}(x,t) = e^{-F(x,t_p)} 2G(x,0) \gamma_{kl}(x,0) \quad + \quad h(t_p) \triangle \gamma_{kl}(t_p) + \quad R_p \tag{3.33}$$

A broad overview of the methodology that can be used to run the present numerical model is shown in Fig.3.2

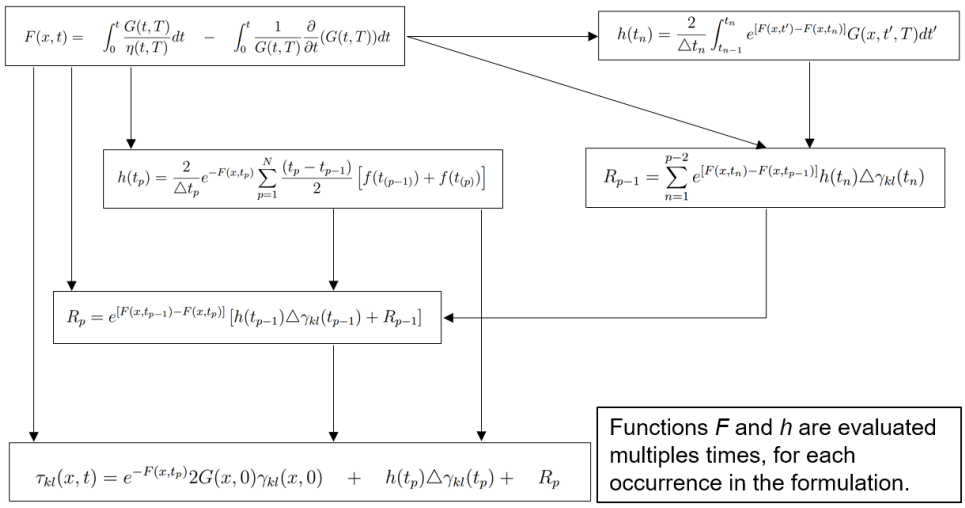

Figure 3.2: Flow chart to a basic numerical model to solve the stress-strain relation for Maxwell model.

However, this method lacks efficiency on account of multiple evaluations of F and h for each of their occurrences in the numerical formulation. While the term, h, is generally evaluated for a relatively small period of time, each evaluation of F at time, t, involves an integration from time, $t = 0$ to $t = t_n$, (where n is the number of step sizes until final time t_p), which becomes progressively more time-consuming to evaluate. For instance, when solving a model with step size $1/10^{th}$ of the time intervals at which stress is being evaluated, there are 35 distinct evaluations of the function F, and 12 distinct evaluations of the function h. In order to address this issue, a computationally less-intensive methodology was developed, as shown in Fig.3.3, wherein F and h are evaluated for the entire range of time

that is of interest. Subsequently, these values are merely extracted for each step in the calculation of stress.

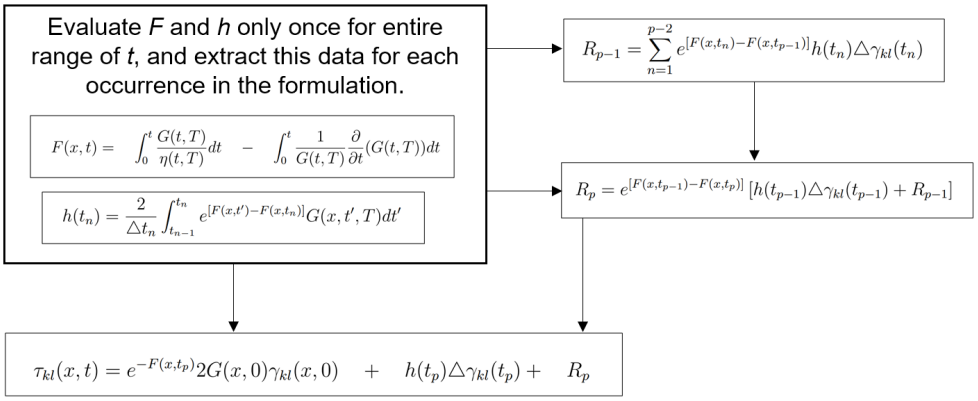

Figure 3.3: Flow chart to an efficient numerical model to solve stress-strain relation for Maxwell model.

3.3 Results and Discussion

The stress-strain relation of a Maxwell model has been solved numerically in Eq.(3.33) for any strain input and material properties changing as curing progresses. The validation for this model is reported below wherein, the strain input and the material properties are taken to be constants as the polymer is considered to be completely cured, i.e ($\alpha = 1$). Using these input parameters, the stress-strain relation has also been solved analytically and the solution from numerical model is verified with analytical equations.

Model Validation

In order to validate the numerical model, the following input parameters are used. The strain input used is a constant strain given as

$$\gamma_{kl}(x,t) = \gamma_0$$

Material properties of the polymer are considered to be constants, i.e.

$$G = G_0 + G_1$$

$$\eta = \eta_0 + \eta_1$$

These properties have been obtained by substituting ($\alpha = 1$) into Eqs.(3.18) and (3.19). These are used under the consideration that the polymer has been fully cured and hence the properties do not vary with time. Results are obtained both numerically and analytically and are plotted in Fig.3.4

The stress-strain relation has been solved numerically

$$\tau_{kl}(x,t) = e^{-F(x,t_p)} 2G(x,0)\gamma_{kl}(x,0) \quad + \quad h(t_p)\triangle\gamma_{kl}(t_p) + \quad R_p \qquad (3.34)$$

For constant strain, since $\gamma_{kl}(t_n) = \gamma_{kl}(x,0) = \gamma_0$, then $\triangle\gamma_{kl}(t_n) = 0$, $\triangle\gamma_{kl}(t_p) = 0$ and $R_p = 0$. Therefore,

$$\tau_{kl} \quad = \quad 2G\gamma_0 e^{-F(x,t_p)} \qquad (3.35)$$

Analytical solution is obtained by carrying out the following derivations. The stress-strain relations for spring and dash-pot for a Maxwell model with constant material properties are given below.

$$\gamma_{kl}^{(G)} = \frac{\tau_{kl}(x,t)}{2G} \tag{3.36}$$

$$\frac{\partial \gamma_{kl}^{(\eta)}}{\partial t} = \frac{\tau_{kl}(x,t)}{2\eta} \tag{3.37}$$

Differentiating Eq.(3.36) and adding it to Eq.(3.37),

$$\frac{\partial \gamma_{kl}}{\partial t} = \frac{\partial}{\partial t}\left(\frac{\tau_{kl}(x,t)}{2G}\right) + \frac{\tau_{kl}(x,t)}{2\eta} \tag{3.38}$$

Since G and η are independent of time, Eq.(3.38) can be re-written as,

$$\frac{\partial \gamma_{kl}}{\partial t} = \frac{1}{2G}\frac{\partial \tau_{kl}(x,t)}{\partial t} + \frac{\tau_{kl}(x,t)}{2\eta} \tag{3.39}$$

Multiplying Eq.(3.39) by $2G$,

$$2G\frac{\partial \gamma_{kl}}{\partial t} = \frac{\partial \tau_{kl}(x,t)}{\partial t} + \frac{\tau_{kl}(x,t)}{\lambda} \tag{3.40}$$

where λ is the relaxation time which can be defined as given below,

$$\frac{1}{\lambda} = \frac{G}{\eta}$$

Initial condition for Maxwell model is,

$$\gamma_{kl}(x,0) = \gamma_{kl}^{G}(x,0) = \frac{\tau_{kl}(x,0)}{2G(0,T)}$$

Using this initial condition, Eq.(3.40) can be solved for τ_{kl} as,

$$\tau_{kl} = 2G\int_0^{t_p} e^{[F(x,t')-F(x,t)]}\frac{\partial \gamma_{kl}(x,t')}{\partial t'}dt' + 2G\gamma_{kl}(x,0)e^{-F(x,t)} \tag{3.41}$$

where,

$$F(x,t) = \int_0^t \frac{dt}{\lambda} = \int_0^t \left(\frac{G}{\eta}\right) dt = \frac{G}{\eta} t \tag{3.42}$$

For constant strain, $\gamma_{kl}(t_n) = \gamma_{kl}(x,0) = \gamma_0$ and $\frac{\partial \gamma_{kl}}{\partial t} = 0$, therefore

$$\tau_{kl} = 2G\gamma_{kl}(x,0)e^{-F(x,t)} \tag{3.43}$$

Using these input parameters, the numerical model is evaluated. The stress is calculated for a temperature of 500K, and inputs for material properties, G and η are $G_0 = 1, G_1 = 5, \eta_0 = 0.5, \eta_1 = 10$. Stress vs time plot has been evaluated for a time period of 5 secs. Eq.(3.43) describes the stress relaxation phenomenon for Maxwell model under constant strain wherein the stresses gradually decreases with time. This phenomenon is shown in Fig. 3.4.

Viscoelastic Polymer with Transient Material Properties

Once the numerical model has been validated, the model can be used to plot the variation of stress for more complex parameters. Consider a constant strain input used for solving the numerical model such that

$$\gamma_{kl}(x,t) = \gamma_0$$

The material properties of the polymer are considered to be time dependent i.e., the properties vary as the cure progresses. In order to obtain these plots,

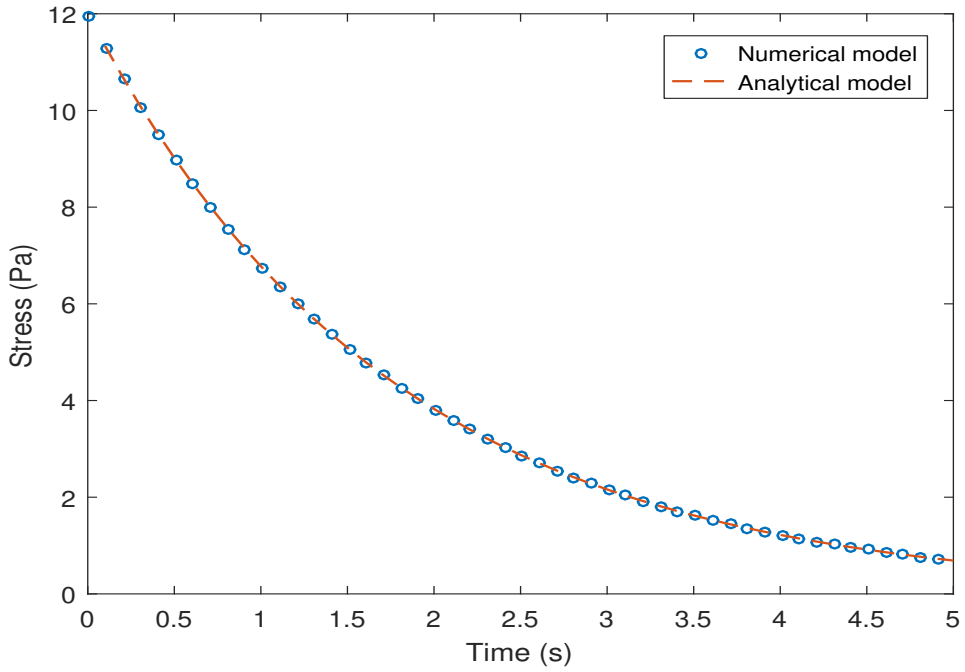

Figure 3.4: Validation of numerical solution for Maxwell model with constant strain input and time independent material properties.

we need to understand the variation of degree of cure as time progresses and this has been solved for 3501-6 resin in Section 2.2 using the Runge-Kutta 4^{th} order method. The results have been plotted in Fig. 3.5 for a temperature value of 500K.

The variation of $G(\alpha, t, T)$ and $\eta(\alpha, t, T)$ with respect to time are as given in Eqs.(3.44) and (3.45). Constant values have been assigned as inputs for material properties in order to plot their variation with time as shown Figs. 3.6 and 3.7 so as to understand their impact on the variation of stress.

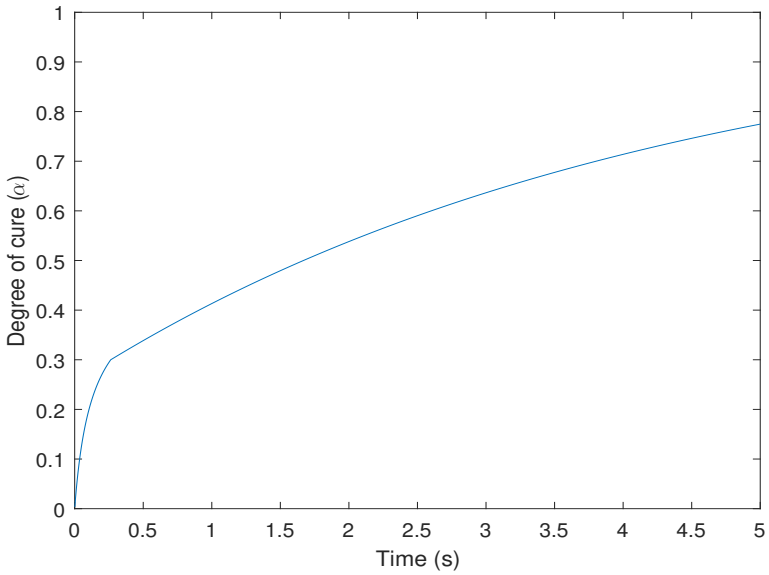

Figure 3.5: Degree of cure vs time for temperature of 500K.

Constant material inputs are given by, $G_0 = 1, G_1 = 5, \eta_0 = 0.5, \eta_1 = 10$.

$$G(\alpha, t, T) = G_0 \ + \ G_1\alpha \tag{3.44}$$

$$\eta(\alpha, t, T) = \eta_0 \ + \ \eta_1\alpha \tag{3.45}$$

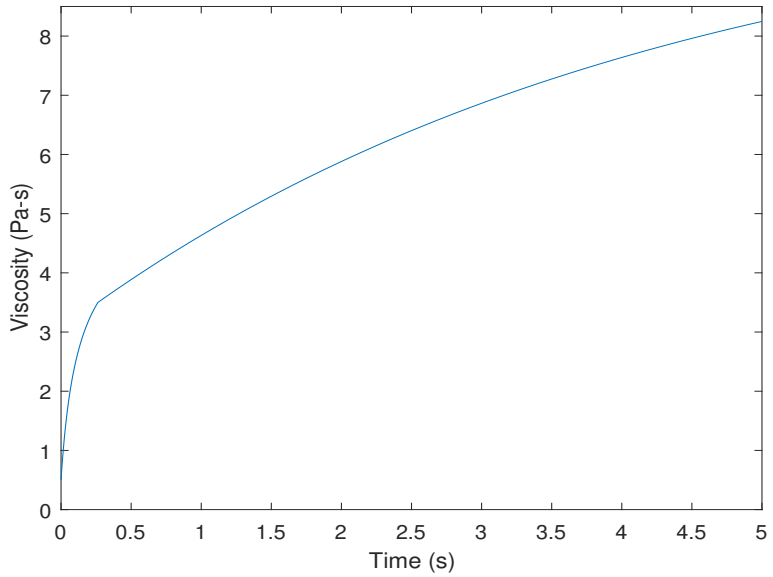

Figure 3.6: Viscosity with time for cure dependent viscoelastic model.

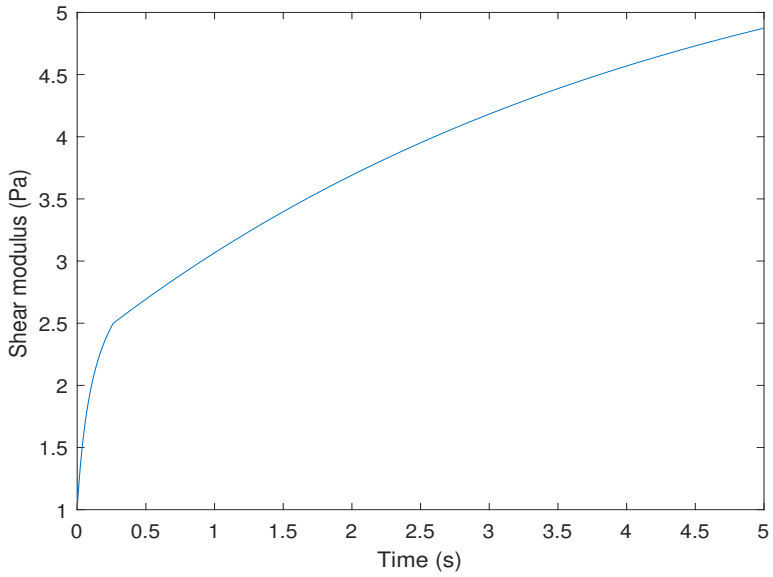

Figure 3.7: Variation of Shear modulus with time for cure dependent viscoelastic model.

The variation of stress with respect to time is as shown in Fig. 3.8. It can be observed that for a constant stress, with material properties increasing, the stresses tend to increase for a short time period and then stress relaxation occurs similar to the validation case from Fig. 3.5.

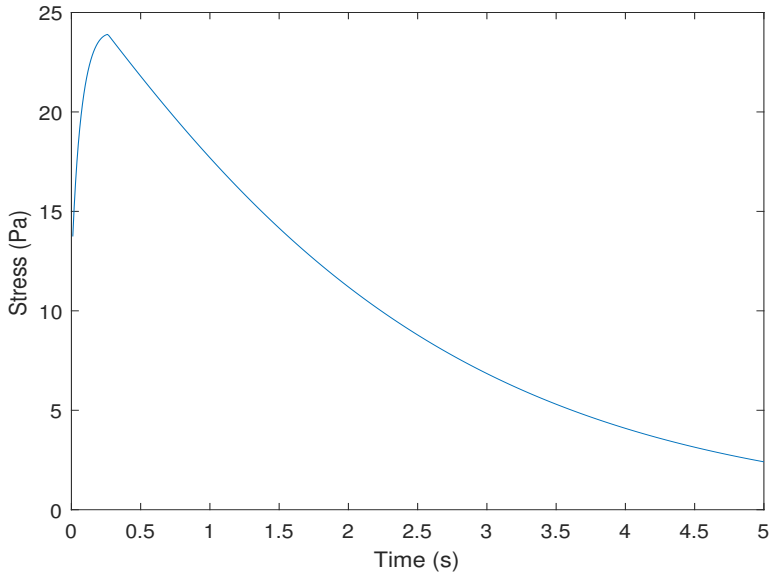

Figure 3.8: Plot of stress τ_{kl} vs time for constant strain input and transient material properties.

4 Generalized Maxwell model (GMM)

4.1 Introduction

The Generalized Maxwell model (GMM) can be formulated as $M + 2$ Maxwell bodies placed in parallel. The first and last Maxwell bodies are degenerate ones such that $\eta_0 = G_{M+1} = \infty$. The load in each Maxwell body is τ_{kl}^m while its deformation is γ_{kl}^m which is equal to the γ_{kl} of entire GMM. Total stress for $M + 2$ Maxwell bodies placed in parallel is given by

$$\tau_{kl}(x,t) = \sum_{m=0}^{M+1} \tau_{kl}^m(x,t) \tag{4.1}$$

The stress-strain relations for degenerate bodies, spring and dash-pot are.

$$\gamma_{kl}^{(G)}(x,t) = \frac{\tau_{kl}(x,t)}{2G(t,T)} \tag{4.2}$$

$$\frac{\partial \gamma_{kl}^{(\eta)}(x,t)}{\partial t} = \frac{\tau_{kl}(x,t)}{2\eta(t,T)} \tag{4.3}$$

Stress-strain relation for a single Maxwell model is derived as,

$$\tau_{kl}(x,t) = 2G(0,T)\gamma_{kl}(x,0)e^{-F(x,t)} + \int_0^{t_p} e^{-[F(x,t)-F(x,t')]} G(t,t',T) \frac{\partial \gamma_{kl}(x,t')}{\partial t'} dt' \tag{4.4}$$

Substituting of Eqs.(4.2), (4.3) and (4.4) into Eq.(4.1) gives,

$$\frac{1}{2}\tau_{kl}(x,t) \quad = \quad G_0(t,T)\gamma_{kl}(x,t) \quad + \quad \eta_{M+1}(t,T)\frac{\partial \gamma_{kl}(x,t)}{\partial t}$$

$$+ \quad \sum_{m=1}^{M} \int_0^{t_p} e^{-[F_m(x,t)-F_m(x,t')]} G_m(t,t',T) \frac{\partial \gamma_{kl}(x,t')}{\partial t'} dt'$$

$$+ \quad \frac{1}{2} \sum_{m=1}^{M} e^{-F_m(x,t)} \tau_{kl}^m(x,0) \tag{4.5}$$

where

$$\tau_{kl}^m(x,0) = 2G_m(0,T)\gamma_{kl}(x,0)$$

For each Maxwell body ($m = 1, 2, ...M$) the relation for relaxation time λ is given by Eq.(4.6) and $F_m(x,t)$ by Eq.(4.7). The GMM contains 2M+2 parameters that characterizes the material properties.

$$\frac{1}{\lambda_m(t,T)} = G_m(t,T) \frac{\partial}{\partial t} \left(\frac{1}{G_m(t,T)} \right) + \frac{G_m(t,T)}{\eta_m(t,T)} \tag{4.6}$$

$$F_m(x,t) = \int_0^t \frac{dt}{\lambda_m(t,T)} \tag{4.7}$$

4.2 Numerical analysis of non-linear Generalized Maxwell model (GMM)

The stress-strain relation in Eq.(4.5) can be numerically solved as follows.

$$\frac{1}{2}\tau_{kl}(x,t) = \quad G_0(t,T)\gamma_{kl}(x,t) \quad + \quad \eta_{M+1}(x,t,T) \frac{\partial \gamma_{kl}(x,t)}{\partial t}$$

$$+ \quad \sum_{m=1}^{M} \sum_{n=1}^{p} \int_{t_{n-1}}^{t_n} e^{-[F_m(x,t_p)-F_m(x,t')]} G_m(t,t',T') \frac{\triangle \gamma_{kl}(t_n)}{\triangle t_n} dt'$$

$$+ \quad \frac{1}{2} \sum_{m=1}^{M} e^{-F_m(x,t)} \tau_{kl}^m(x,0) \tag{4.8}$$

Assuming that $\triangle\gamma_{kl}(t_n)$ is constant over $\triangle t_n$, then

$$\frac{1}{2}\tau_{kl}(x,t) = \quad G_0(t,T)\gamma_{kl}(x,t) \quad + \quad \eta_{M+1}(x,t,T)\frac{\partial\gamma_{kl}(x,t)}{\partial t}$$
$$+ \quad \sum_{m=1}^{M}\sum_{n=1}^{p}\int_{t_{n-1}}^{t_n} e^{-[F_m(x,t_p)-F_m(x,t')]}G_m(t,t',T)dt'\frac{\triangle\gamma_{kl}(t_n)}{\triangle t_n}$$
$$+ \quad \frac{1}{2}\sum_{m=1}^{M} e^{-F_m(x,t)}\tau_{kl}^m(x,0) \tag{4.9}$$

Adding and subtracting $F_m(x,t_n)$ to $[F_m(x,t') - F_m(x,t_p)]$, Eq.4.9 can be re-written as

$$\frac{1}{2}\tau_{kl}(x,t) = \quad G_0(x,t,T)\gamma_{kl}(x,t) \quad + \quad \eta_{M+1}(x,t,T)\frac{\partial\gamma_{kl}(x,t)}{\partial t}$$
$$+ \quad \sum_{m=1}^{M}\sum_{n=1}^{p}\int_{t_{n-1}}^{t_n} e^{[F_m(x,t')-F_m(x,t_p)+F_m(x,t_n)-F_m(x,t_n)]}G_m(x,t',T')dt'\frac{\triangle\gamma_{kl}(t_n)}{\triangle t_n}$$
$$+ \quad \frac{1}{2}\sum_{m=1}^{M} e^{-F_m(x,t)}\tau_{kl}^m(x,0)$$

$$= \quad G_0(x,t,T)\gamma_{kl}(x,t) \quad + \quad \eta_{M+1}(x,t,T)\frac{\partial\gamma_{kl}(x,t)}{\partial t}$$
$$+ \quad \sum_{m=1}^{M}\sum_{n=1}^{p} e^{[F_m(x,t_n)-F_m(x,t_p)]}\int_{t_{n-1}}^{t_n}\sum_{m=1}^{M} e^{[F_m(x,t')-F_m(x,t_n)]}G_m(x,t',T')dt'\frac{\triangle\gamma_{kl}(t_n)}{\triangle t_n}$$
$$+ \quad \frac{1}{2}\sum_{m=1}^{M} e^{-F_m(x,t)}\tau_{kl}^m(x,0) \tag{4.10}$$

Then,

$$\frac{1}{2}\tau_{kl}(x,t) = \quad G_0(x,t,T)\gamma_{kl}(x,t) \quad + \quad \eta_{M+1}(x,t,T)\frac{\partial\gamma_{kl}(x,t)}{\partial t}$$
$$+ \quad \sum_{m=1}^{M}\int_{t_{p-1}}^{t_p} e^{[F_m(x,t')-F_m(x,t_p)]}G_m(x,t',T)dt'\frac{\triangle\gamma_{kl}(t_p)}{\triangle t_p}$$

$$+ \quad \sum_{m=1}^{M}\sum_{n=1}^{p-1} e^{[F_m(x,t_n)-F_m(x,t_p)]}\int_{t_{n-1}}^{t_n}\sum_{m=1}^{M} e^{[F_m(x,t')-F_m(x,t_n)]}G_m(x,t',T)dt'\frac{\triangle\gamma_{kl}(t_n)}{\triangle t_n}$$

$$+ \quad \frac{1}{2}\sum_{m=1}^{M} e^{-F_m(x,t)}\tau_{kl}^{m}(x,0) \tag{4.11}$$

Let us define h_m as

$$h_m(t_p) = \frac{1}{\triangle t_p}\int_{t_{p-1}}^{t_p}\sum_{m=1}^{M} e^{[F_m(x,t')-F_m(x,t_p)]}G_m(x,t',T)dt' \tag{4.12}$$

$$h_m(t_n) = \frac{1}{\triangle t_n}\int_{t_{n-1}}^{t_n}\sum_{m=1}^{M} e^{[F_m(x,t')-F_m(x,t_n)]}G_m(x,t',T)dt' \tag{4.13}$$

Therefore,

$$\frac{1}{2}\tau_{kl}(x,t) = \quad G_0(x,t,T)\gamma_{kl}(x,t) \quad + \quad \eta_{M+1}(x,t,T)\frac{\partial\gamma_{kl}(x,t)}{\partial t}$$

$$+ \quad h_m(t_p)\triangle\gamma_{kl}(t_p)$$

$$+ \quad \sum_{n=1}^{p-1}\sum_{m=1}^{M} e^{[F_m(x,t_n)-F_m(x,t_p)]}h_m(t_n)\triangle\gamma_{kl}(t_n)$$

$$+ \quad \frac{1}{2}\sum_{m=1}^{M} e^{-F_m(x,t)}\tau_{kl}^{m}(x,0) \tag{4.14}$$

Let us define $R_{p,m}$ as

$$R_{p,m} = \sum_{n=1}^{p-1}\sum_{m=1}^{M} e^{[F_m(x,t_n)-F_m(x,t_p)]}h_m(t_n)\triangle\gamma_{kl}(t_n) \tag{4.15}$$

Then we have

$$R_{p-1,m} = \sum_{n=1}^{p-2}\sum_{m=1}^{M} e^{[F_m(x,t_n)-F_m(x,t_{p-1})]}h_m(t_n)\triangle\gamma_{kl}(t_n) \tag{4.16}$$

$R_{p,m}$ can be re-written as

$$R_{p,m} = \sum_{m=1}^{M} e^{[F_m(x,t_{p-1})-F_m(x,t_p)]} h_m(t_{p-1}) \triangle \gamma_{kl}(t_{p-1}) + \sum_{n=1}^{p-2} \sum_{m=1}^{M} e^{[F_m(x,t_n)-F_m(x,t_p)]} h_m(t_n) \triangle \gamma_{kl}(t_n) \tag{4.17}$$

$$= \sum_{m=1}^{M} e^{[F_m(x,t_{p-1})-F_m(x,t_p)]} h_m(t_{p-1}) \triangle \gamma_{kl}(t_{p-1}) + \sum_{m=1}^{M} e^{[F_m(x,t_{p-1})-F_m(x,t_p)]} \sum_{n=1}^{p-2} \sum_{m=1}^{M} e^{[F_m(x,t_n)-F_m(x,t_{p-1})]} h(t_n) \triangle \gamma_{kl}(t_n) \tag{4.18}$$

Therefore,

$$R_{p,m} = \sum_{m=1}^{M} e^{[F_m(x,t_{p-1})-F_m(x,t_p)]} \left[h_m(t_{p-1}) \triangle \gamma_{kl}(t_{p-1}) + R_{p-1,m} \right] \tag{4.19}$$

Then,

$$\frac{1}{2}\tau_{kl}(x,t) = G_0(x,t,T)\gamma_{kl}(x,t) + \eta_{M+1}(x,t,T)\frac{\partial \gamma_{kl}(x,t)}{\partial t} + h_m(t_p)\triangle\gamma_{kl}(t_p) + R_{p,m} + \frac{1}{2}\sum_{m=1}^{M} e^{-F_m(x,t)} \tau_{kl}^{m}(x,0) \tag{4.20}$$

4.3 Numerical model validation

Validation of numerical solution for Generalized Maxwell model is carried out using a sample viscoelastic model as shown in Fig.4.1, wherein, $m = 1, 2$. The stress-strain relations for the fully cured polymer with constant

material properties are computed numerically using Eq.(4.20) for a constant strain input and the result is compared to the analytical solution.

$$G_m = G_{0m} + G_{1m} \tag{4.21}$$

$$\eta_m = \eta_{0m} + \eta_{1m}. \tag{4.22}$$

$$F_m(x,t) = \int_0^t \frac{dt}{\lambda_m} = \int_0^t \left(\frac{G_m}{\eta_m}\right) dt = \frac{G_m}{\eta_m} t \tag{4.23}$$

Also strain input is given as,

$$\gamma_{kl} = \gamma_0$$

Therefore,

$$\triangle\gamma_{kl} = 0 \tag{4.24}$$

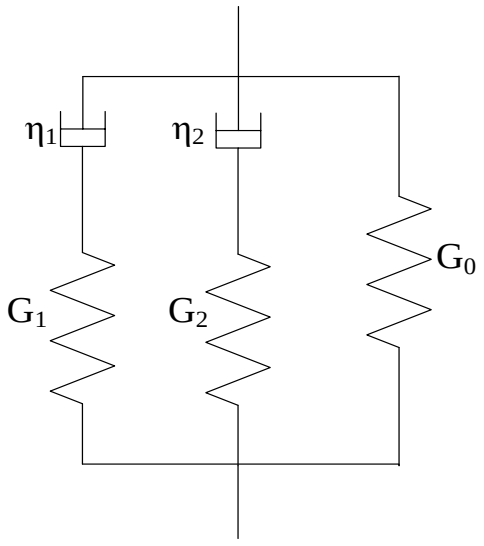

Figure 4.1: Sample viscoelastic model to validate numerical solution for GMM .

Stress is calculated numerically using Eq.(4.20) as

$$\frac{1}{2}\tau_{kl}(x,t) = \quad G_0\gamma_0 + \quad \frac{1}{2}\sum_{m=1}^{2} e^{-F_m(x,t)}\tau_{kl}^m(x,0)$$

$$+ \quad h_m(t_p)\triangle\gamma_{kl}(t_p) \quad + \quad R_{p,m} \tag{4.25}$$

Substituting the above mentioned input parameters into Eq.(4.25),

$$\tau_{kl}(x,t) = \quad 2G_0\gamma_0 + \quad \sum_{m=1}^{2} e^{-F_m(x,t)}\tau_{kl}^m(x,0) \tag{4.26}$$

where

$$\tau_{kl}^1(x,0) = 2(G_{01} + G_{11})\gamma_0$$

$$\tau_{kl}^2(x,0) = 2(G_{02} + G_{12})\gamma_0 \tag{4.27}$$

The analytical solution to the sample model in Fig.4.1 can be obtained by considering it as a GMM consisting of two Maxwell models (M=2) and a spring (G_0) connected in parallel. The strain in each model is equal to the total strain and is given as

$$\gamma_{kl} = \gamma_{kl}^1 = \gamma_{kl}^2 = \gamma_{kl}^0 \tag{4.28}$$

Let τ_{kl}^1, τ_{kl}^2 be the stresses in the Maxwell models and τ_{kl}^3 is the stress induced in the spring, then total stresses can be calculated as,

$$\tau_{kl} = \tau_{kl}^1 + \tau_{kl}^2 + \tau_{kl}^0 \tag{4.29}$$

where

$$\tau_{kl}^1 = 2G_1\gamma_{kl}(x,0)e^{-F_1(x,t)} \tag{4.30}$$

$$\tau_{kl}^2 = 2G_2\gamma_{kl}(x,0)e^{-F_2(x,t)} \tag{4.31}$$

$$\tau_{kl}^0 = 2G_0\gamma_{kl}(x,0) \tag{4.32}$$

Using Eqs.(4.21), (4.22) and (4.23),

$$F_1(x,t) = \frac{G_1}{\eta_1}t = \frac{(G_{01}+G_{11})}{(\eta_{01}+\eta_{11})}t$$

$$F_2(x,t) = \frac{G_2}{\eta_2}t = \frac{(G_{02}+G_{12})}{(\eta_{02}+\eta_{12})}t$$

Therefore,

$$\tau_{kl} = 2G_1\gamma_{kl}(x,0)e^{-F_1(x,t)} + 2G_2\gamma_{kl}(x,0)e^{-F_2(x,t)} + 2G_0\gamma_{kl}(x,0) \tag{4.33}$$

In order to plot stress-time graphs for both numerical and analytical solutions, sample values are given for material properties as shown below,

For the first Maxwell body,

$$m = 1, G_{01} = 10, G_{11} = 3, \eta_{01} = 5, \eta_{11} = 2 \tag{4.34}$$

For the second Maxwell body,

$$m = 2, G_{02} = 5, G_{12} = 2, \eta_{02} = 4, \eta_{12} = 1 \tag{4.35}$$

The spring constant for a degenerate spring is

$$G_0 = 3 \tag{4.36}$$

The stresses thus obtained numerically are compared with the stress-strain relations evaluated theoretically for constant strain ($\gamma_0 = 1$) and

results are plotted in Fig.4.2. It is observed that the sample model undergoes stress-relaxation when a constant strain is applied at a temperature of 500K and it can be seen that the stresses decreases gradually with time.

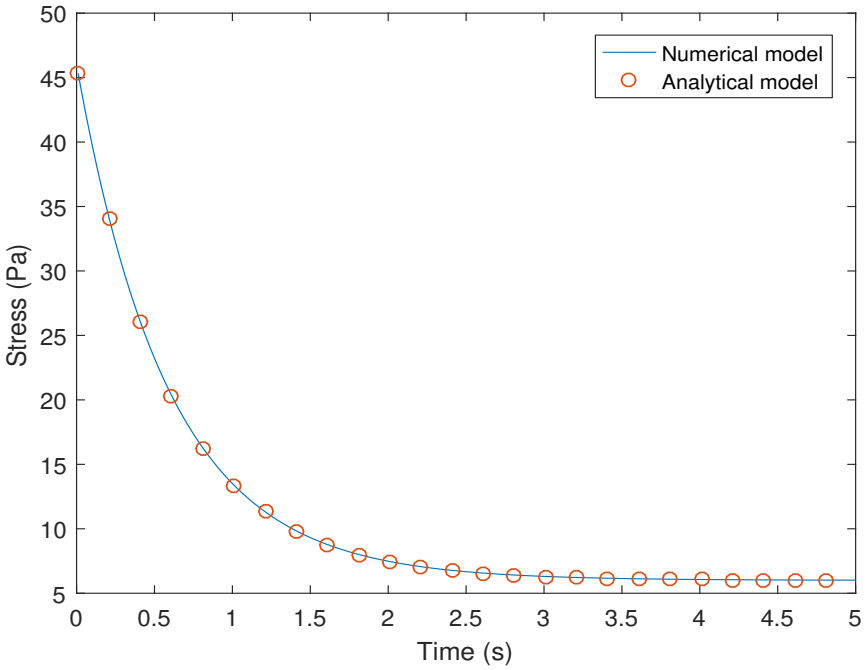

Figure 4.2: Validation of numerical model using analytical solution for sample GMM.

4.4 Characterization of sample model with cure dependent material properties

Once the sample model in Fig.4.1 has been validated using numerical model, it can now be used to evaluate the stress induced in the polymer with cure

dependent material properties as

$$G_m = G_{0m} + G_{1m}\alpha \tag{4.37}$$

$$\eta_m = \eta_{0m} + \eta_{1m}\alpha \tag{4.38}$$

Variation of degree of cure α with time has been calculated in Section 2.2 based on cure kinetic relations for 3501-6 resin and is plotted in Fig. 4.3 for a temperature of 500K.

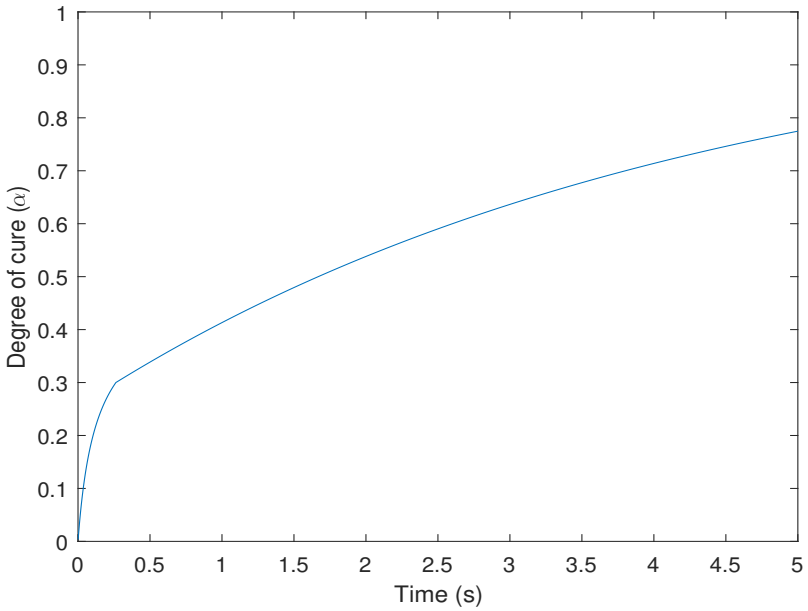

Figure 4.3: Variation of degree of cure with time for a temperature input of 500K.

For $\alpha \leq 0.3$,

$$t = \frac{-1}{(K_1+K_2)(B-1)}\ \ln|1-\alpha| + \frac{1}{(K_2B+K_1)(B-1)}\ \ln|1-\frac{\alpha}{B}| + \frac{K_2}{(K_1+K_2)(K_2B+K_1)}\ \ln|1+\frac{K_2\alpha}{K_1}|$$

For $\alpha > 0.3$, we have

$$t = -\frac{1}{K_3} \ln \frac{(1-\alpha)}{0.7} + t_c$$

where

$$t_c = \frac{-1}{(K_1+K_2)(B-1)} \ln(0.7) + \frac{1}{(K_2B+K_1)(B-1)} \ln|1 - \frac{0.3}{B}|$$
$$+ \frac{K_2}{(K_1+K_2)(K_2B+K_1)} \ln|1 + \frac{0.3K_2}{K_1}|$$

The strain input in this case is also constant given by, $\gamma_{kl} = \gamma_0$.

For the first Maxwell body,

$$m = 1, G_{01} = 10, G_{11} = 3, \eta_{01} = 5, \eta_{11} = 2 \tag{4.39}$$

For the second Maxwell body, input parameters are

$$m = 2, G_{02} = 5, G_{12} = 2, \eta_{02} = 4, \eta_{12} = 1 \tag{4.40}$$

The spring constant for a degenerate spring, input parameters are

$$G_0 = 3 \tag{4.41}$$

Figs. 4.4 and 4.5 show the variation of shear modulus G and modulus of viscosity η with time for all the components connected parallel in the sample model.

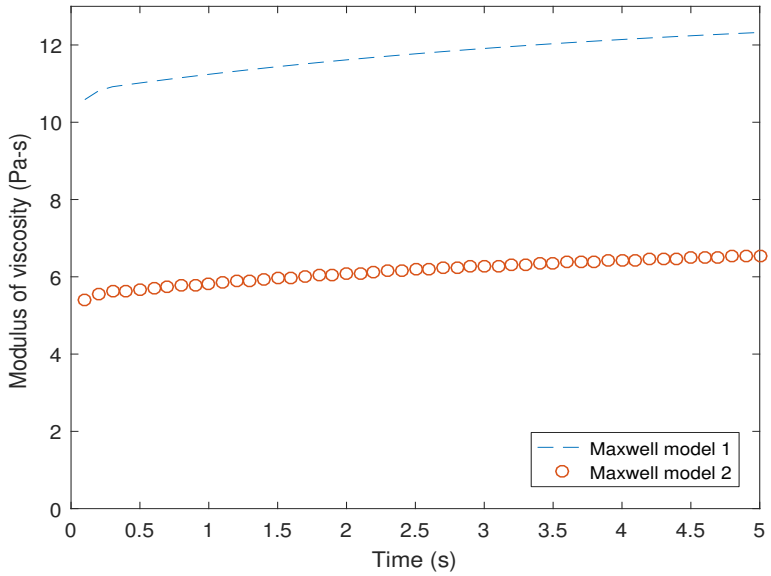

Figure 4.4: Modulus of viscosity vs time for Maxwell models 1 and 2.

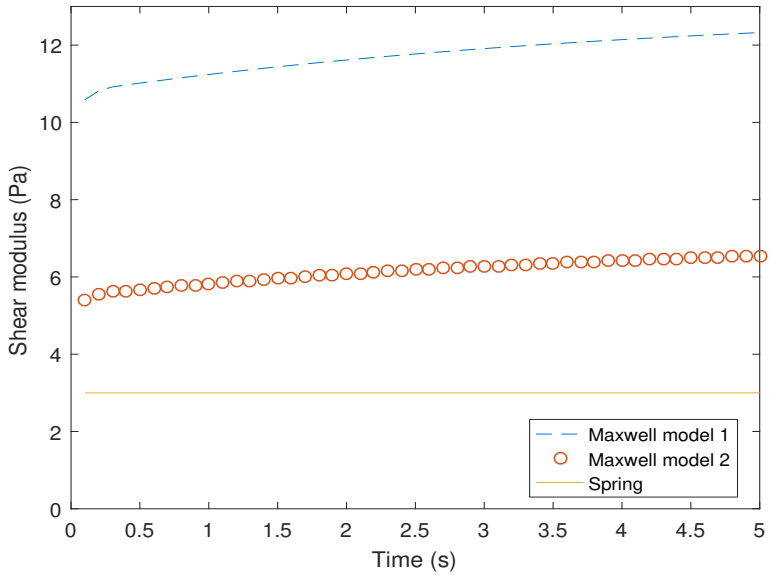

Figure 4.5: Plot of Shear modulus vs time for Maxwell models 1, 2, and Spring component.

Individual stresses in the Maxwell models as well as the spring component connected in parallel are plotted in Fig.4.6. It can be noted that

while the stress in the spring component increases linearly, Maxwell model stresses initially tend to decrease and then increase. The stresses in Maxwell model 1 is higher than Maxwell model 2 and spring component due to high values of material properties as seen in Fig.4.4 and 4.5. Stresses for the GMM sample model as a whole is poltted in Fig.4.7.At time $t = 0$, stress was very high due to initial strain, γ_0. Then as time progressed, stresses seem to be reduced and then eventually increase.

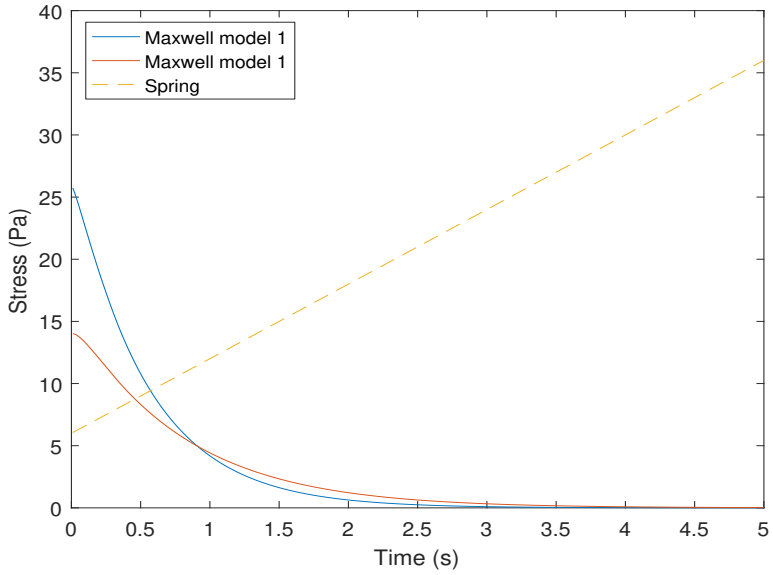

Figure 4.6: Stress-time plot of individual components for cure-dependent material properties.

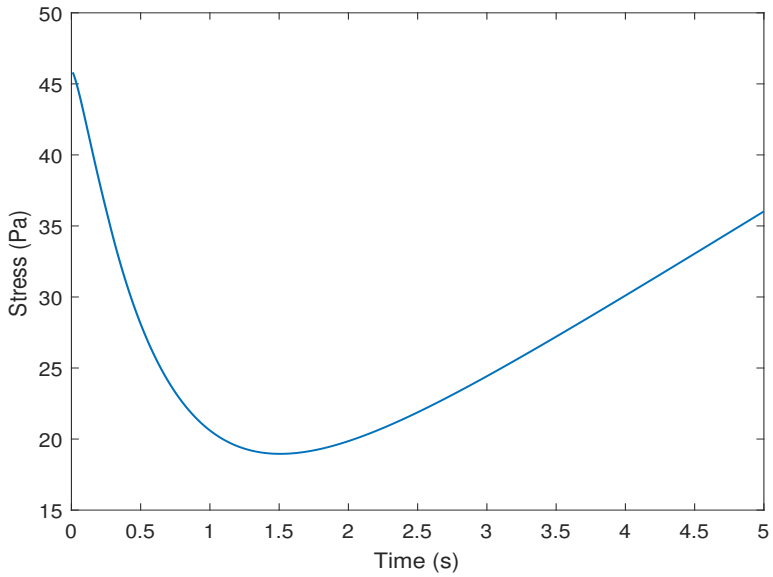

Figure 4.7: Stress-time plot for cure-dependent material properties.

5 Dissipation Energy

5.1 Dissipation energy for Single Maxwell model

During the deformation of a viscoelastic polymer, part of the total work of deformation is stored elastically, whereas, remainder is dissipated as heat through viscous losses. It is of great interest to determine this energy dissipated as it can create thermal stresses in the material that may affect the overall efficiency of the electronic package in which it is being used. By definition, energy is dissipated in the dashpot alone and hence, dissipation energy is given by,

$$W^d = \int_0^t \tau_{kl}^{\eta}(x,t)\frac{\partial \gamma_{kl}^{\eta}(x,t)}{\partial t}dt \tag{5.1}$$

The stress-strain relation for a dash-pot in Maxwell model is as

$$\frac{\partial \gamma_{kl}^{\eta}(x,t)}{\partial t} = \frac{\tau_{kl}(x,t)}{2\eta(t,T)} \tag{5.2}$$

Substituting Eq.(5.2) into Eq.(5.1),

$$W^d = \int_0^t \frac{[\tau_{kl}(x,t)]^2}{2\eta(t,T)}dt \tag{5.3}$$

where

$$\eta(t,T) = \eta_0 + \eta_1\alpha \tag{5.4}$$

$$\tau_{kl}(x,t) = 2G(0,T)\gamma_{kl}(x,0)e^{-F(x,t)} + 2\int_0^{t_p} e^{[F(x,t')-F(x,t)]}G(T,t,t')\frac{\partial \gamma_{kl}(x,t')}{\partial t'}dt' \tag{5.5}$$

Therefore,

$$W^d = \int_0^{t_p} \frac{[2G(0,T)\gamma_{kl}(x,0)e^{-F(x,t)} + 2\int_0^{t_p} e^{[F(x,t')-F(x,t)]}G(T,t,t')\frac{\partial\gamma_{kl}(x,t')}{\partial t'}dt']^2}{2[\eta_0 + \eta_1(\alpha)]}dt \tag{5.6}$$

The numerical solution of stress for Maxwell model was derived earlier as

$$\tau_{kl}(x,t) = e^{-F(x,t_p)}2G(x,0)\gamma_{kl}(x,0) \quad + \quad h(t_p)\triangle\gamma_{kl}(t_p) + R_p \tag{5.7}$$

Then,

$$W^d = \int_0^{t_p} \frac{[e^{-F(x,t_p)}2G(x,0)\gamma_{kl}(x,0) \quad + \quad h(t_p)\triangle\gamma_{kl}(t_p) + R_p]^2}{2[\eta_0 + \eta_1\alpha]}dt \tag{5.8}$$

The definite integral for dissipation energy in Eq.(5.8) is evaluated using the trapezoidal method of numerical integration, wherein, area under the curve which is obtained by plotting $f(t)$ w.r.t time, t is approximated as a trapezoid and calculated.

$$W^d = \int_0^{t_p} f(t)dt = \frac{(t_p - 0)}{2}\left[f(0) + f(t_{(p)})\right] \tag{5.9}$$

The results of the integral can be better approximated using composite trapezoidal rule by partitioning the integration interval (into N parts) and applying trapezoidal rule to each sub-interval and summing the results.

Then,

$$W^d = \frac{t_1 - t_0}{2} f(t_0) + \sum_{N=1}^{p-1} \frac{h_j + h_{j+1}}{2} f(t_j) + \frac{t_p - t_{p-1}}{2} f(t_p) \tag{5.10}$$

where,

$$h_j = t_j - t_{j-1}$$

$$h_{j+1} = t_{j+1} - t_j$$

Validation of numerical model

Validation of the numerical method for determining dissipation energy is carried out for a single Maxwell model with constant strain input and constant material properties. The strain input is constant and given by, $\gamma_{kl}(x,0) = \gamma_0 = 1$,then $\triangle\gamma = 0$, the stress-strain relation obtained numerically and analytically from Eqs.(5.5) and (5.6) can be modified for the input parameters are is given as,

$$\tau_{kl}(x,t) = e^{-F(x,t)} 2G(0,T)\gamma_0 \tag{5.11}$$

For constant material properties, $\alpha = 1$, therefore,

$$\eta(t,T) = \eta_0 + \eta_1 \tag{5.12}$$

$$G(t,T) = G_0 + G_1 \tag{5.13}$$

$$\lambda = \frac{\eta(t,T)}{G(t,T)} \tag{5.14}$$

$$F(x,t) = \int_0^t \frac{dt}{\lambda(t,T)} = \frac{t}{\lambda(t,T)} \tag{5.15}$$

Substituting Eqs.(5.11), (5.12), (5.13) and (5.15) into Eq.(5.3), analytical solution is obtained as,

$$W^d = \int_0^{t_p} \frac{[e^{-F(x,t)} 2G(x,0)\gamma_0]^2}{2[\eta_0 + \eta_1]} dt$$

$$= \frac{2G_0^2\gamma_0^2}{\eta_0 + \eta_1} \int_0^{t_p} \exp\left(\frac{-2t}{\lambda(t,T)}\right) dt$$

$$= \frac{G_0^2\gamma_0^2}{G_0 + G_1} \left[1 - \exp\left(\frac{-2t}{\lambda(t,T)}\right)\right] \tag{5.16}$$

The numerical solution is obtained by substituting Eqs. (5.11) and (5.12) into Eq.(5.6) and solving the integral using trapezoidal rule. Fig.5.1 gives a plot comparing the analytical and numerical solution for dissipation energy of Maxwell model with constant strain input and constant material properties G and η, where $G_0 = 1, G_1 = 5, \eta_0 = 0.5, \eta_1 = 10$. Dissipation energy vs time plot has been evaluated for a time period of 5s for a temperature of 500K. From the plot, it can be observed that the numerical solution coincides with analytical results and hence the numerical model for dissipation energy can be considered to be validated.

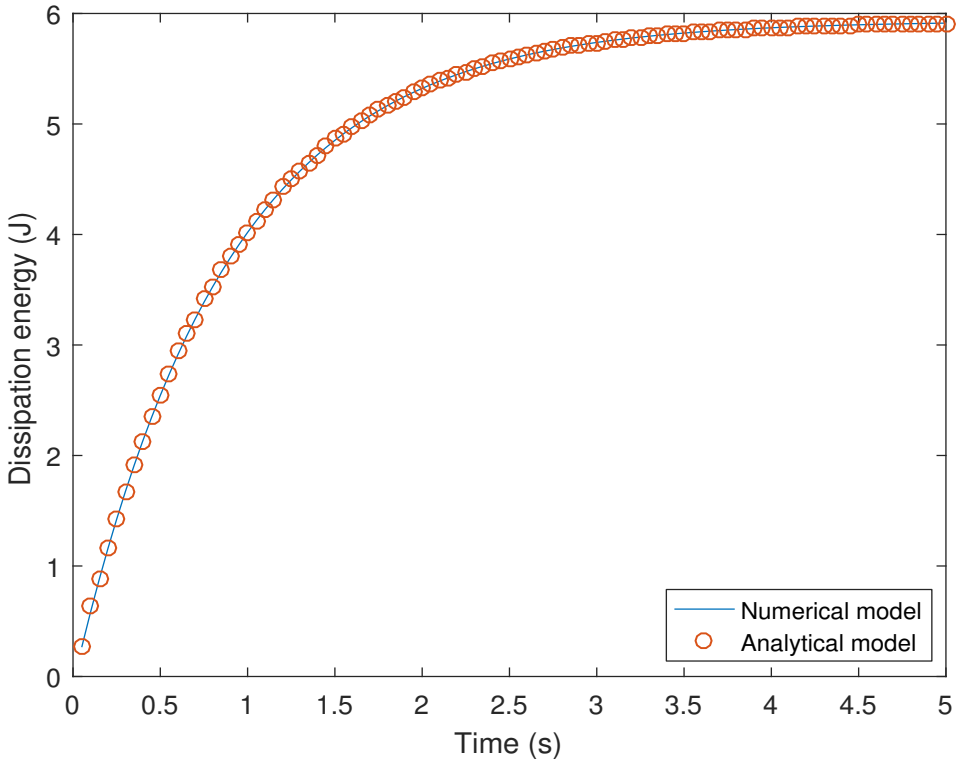

Figure 5.1: Validation of numerical model for dissipation energy calculation of Maxwell model with constant material properties (and constant strain input).

DE plot for polymers with transient material properties

Once the model has been validated for a simple case, it can be used to characterize polymers whose properties are cure dependent. The strain input is constant and given by, $\gamma_{kl}(x,0) = \gamma_0 = 1$,then $\triangle\gamma = 0$. Inputs for material properties, $G(\alpha,t,T)$ and $\eta(\alpha,t,T)$ are $G_0 = 1, G_1 = 5, \eta_0 = 0.5, \eta_1 = 10$. The variation of $G(\alpha,t,T)$ and $\eta(\alpha,t,T)$ with respect to time,

in terms of degree of cure, is given by

$$G = G_0 + G_1\ \alpha$$

$$\eta = \eta_0 + \eta_1\ \alpha$$

Variation of degree of cure as time progresses has been solved for 3501-6 resin in Section 2.2 using the Runge Kutta 4^{th} order method and the results are as given below

For $\alpha \leq 0.3$,

$$t = \frac{-1}{(K_1 + K_2)(B-1)}\ \ln|1-\alpha| + \frac{1}{(K_2B + K_1)(B-1)}\ \ln|1 - \frac{\alpha}{B}|$$

$$+\frac{K_2}{(K_1 + K_2)(K_2B + K_1)}\ \ln|1 + \frac{K_2\alpha}{K_1}|$$

For $\alpha > 0.3$,

$$t = -\frac{1}{K_3}\ln\frac{(1-\alpha)}{0.7} + t_c$$

where

$$t_c = \frac{-1}{(K_1 + K_2)(B-1)}\ln(0.7) + \frac{1}{(K_2B + K_1)(B-1)}\ln|1 - \frac{0.3}{B}|$$
$$+\frac{K_2}{(K_1 + K_2)(K_2B + K_1)}\ln|1 + \frac{0.3K_2}{K_1}|$$

Dissipation energy is calculated as,

$$W^d = \int_0^t \frac{[\tau_{kl}(x,t)]^2}{2\eta(t,T)}dt$$

Dissipation energy has been calculated numerically and plotted as in Fig.5.2.

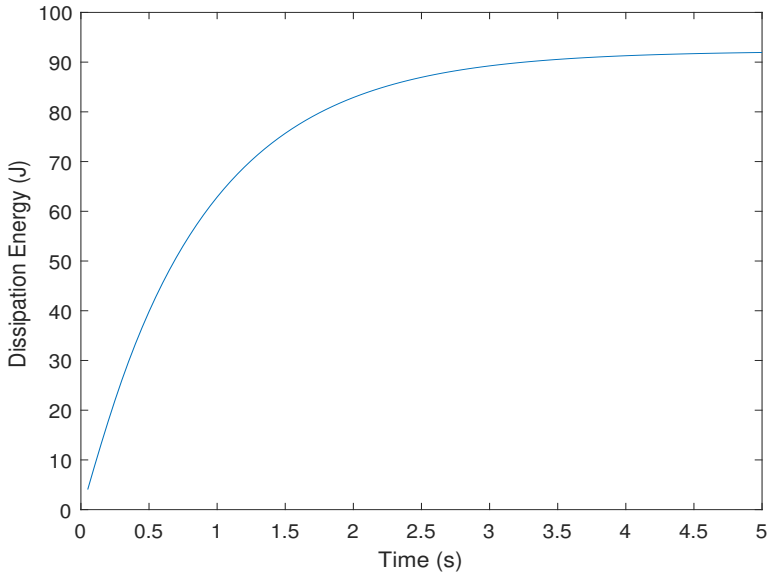

Figure 5.2: Plot of dissipation energy vs time for polymer with transient material properties (and constant strain input).

5.2 Dissipation energy of Generalized Maxwell model (GMM)

Numerical analysis of stress-strain characteristics have been analyzed in Section 4.2. A sample viscoelastic model was chosen as shown in Fig.4.1. This model was already validated for stress-time characteristics using the numerical model for constant strain input and constant material properties, as shown in Fig.4.2. Here, the dissipation energy is validated against analytical solution for the same input parameters. The result is shown

in Fig.5.3 and as can be seen, a good agreement is obtained between the numerical model and analytical solution.

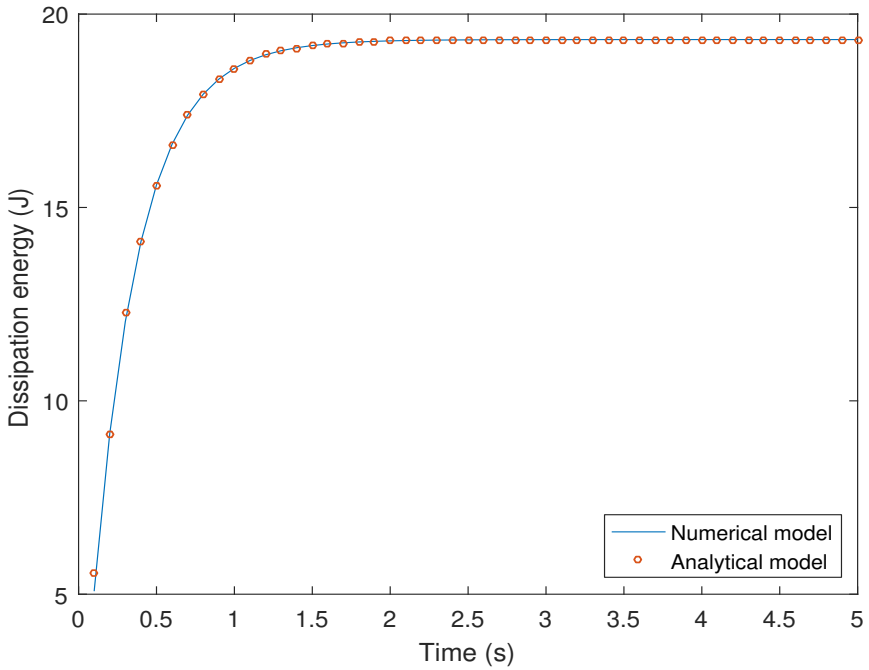

Figure 5.3: Plot of dissipation energy vs time for constant material properties (and constant strain input).

Subsequently, the validated numerical model is now used to simulate the GMM case for transient material properties with constant strain input loading.

$$\gamma_{kl} = \gamma_0$$

These results are reported in Fig.5.4, and as seen therein, dissipation energy increases with time. The variation of material properties are given

as,

$$G_m = G_{0m} + G_{1m}\alpha \tag{5.17}$$

$$\eta_m = \eta_{0m} + \eta_{1m}\alpha \tag{5.18}$$

Variation of degree of cure α with time has been calculated in Section 2.2 based on cure kinetic relations for 3501-6 resin for a temperature of 500K.

For the first Maxwell body,

$$m = 1, G_{01} = 10, G_{11} = 3, \eta_{01} = 5, \eta_{11} = 2 \tag{5.19}$$

For the second Maxwell body,

$$m = 2, G_{02} = 5, G_{12} = 2, \eta_{02} = 4, \eta_{12} = 1 \tag{5.20}$$

The spring constant for a degenerate spring,

$$G_0 = 3 \tag{5.21}$$

The variation of dissipation energy with time for the sample model with transient material properties is as shown in Fig.5.4.

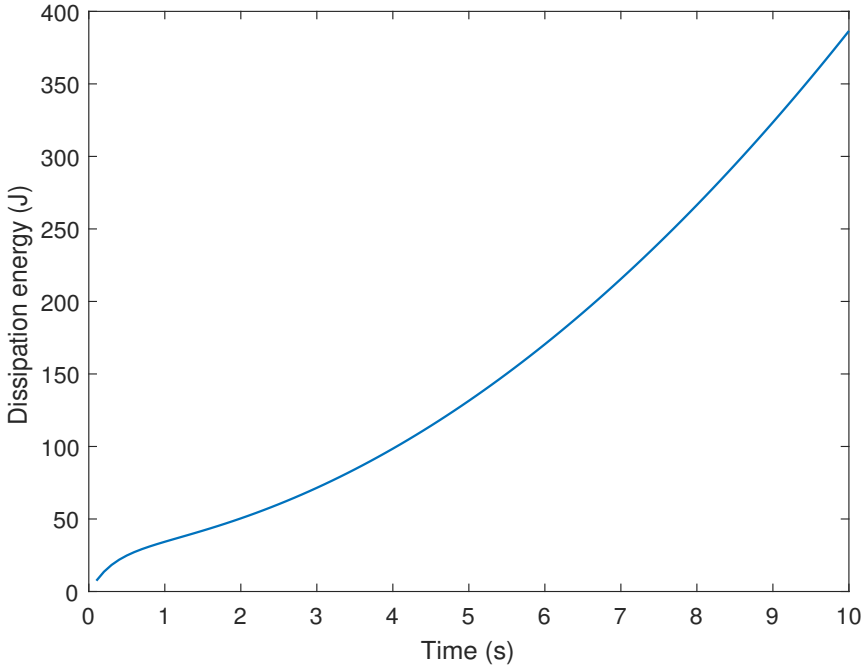

Figure 5.4: Plot of DE vs time for linear strain input using varying material properties (and constant strain input).

6 Characterization of 3501-6 resin

Previously, in Section.2, an assumption was made for simplicity, wherein material properties for 3501-6 resin, $G(\alpha)$ and $\eta(\alpha)$ were assumed to vary linearly with degree of cure and stress-strain characteristics were plotted accordingly. In this study, actual material properties are chosen for modeling the stress-stain characteristics based upon the experimental data.

The variation of shear modulus $G(\alpha)$ with alpha is given in Eq.(6.1) which is obtained from study by Adolf and Martin, (1996), wherein $G^f(x,t)$ is the shear modulus of a fully cured resin, α_g is the degree of cure at gelation point for a particular resin, α_f is the value of α for a fully cured resin.

For 3501-6 resin, $G^f(x,t) = 1065Pa$, resin gelation point α_g has been calculated by Lee et al.(1982) and found to be, 0.5 and maximum value of degree of cure, $\alpha_f = 1$.

$$G(\alpha) = G^f(x,t)\left(\frac{\alpha^2 - \alpha_g^2}{\alpha_f^2 - \alpha_g^2}\right)^{8/3} \tag{6.1}$$

The variation of $\eta(\alpha)$ with degree of cure for 3501-6 resin is given by Eq.(6.2), which is obtained from the study by Lee et al. (1982) wherein $\eta_\infty = 7.93 \times 10^{-14}$ Pa.s, $U = 9.08 \times 10^4$J/mol, $R = 8.314$J/mol-K, T-

temperature, $K = 14.1 \pm 1.2$.

$$\eta(x,t) = \eta_\infty \exp\left(\frac{U}{RT} + K\alpha\right) \tag{6.2}$$

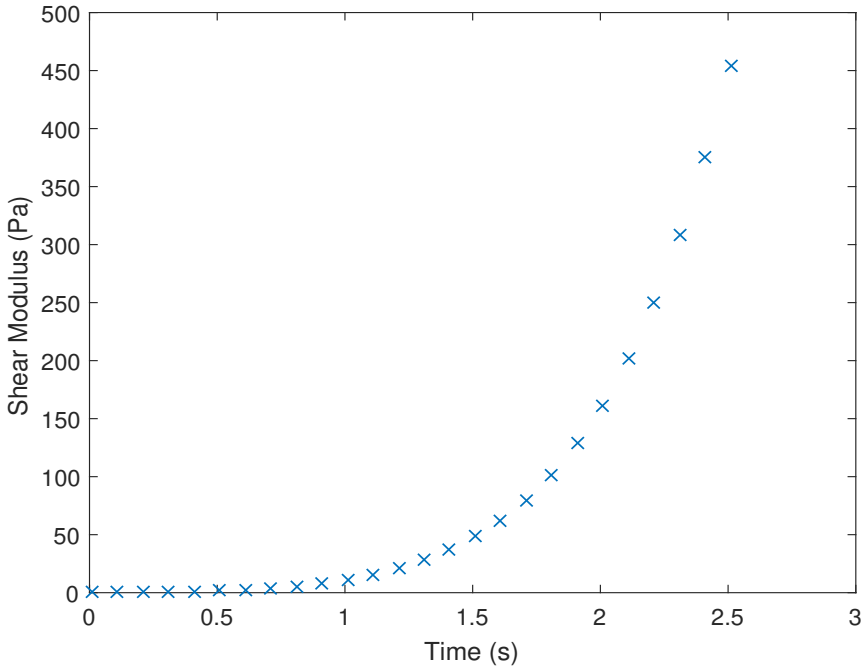

Figure 6.1: Variation of shear modulus with respect to time for 3501-6 resin during curing.

In order to plot the variation of G and η with respect to time as shown in Figs. 6.1 and 6.2, a relation needs to be obtained between degree of cure (α) and time. This has been obtained in Section 2.2 for 3501-6 resin using Runge Kutta 4^{th} order method and the results are as given below,

For $\alpha \leq 0.3$,

$$t = \frac{-1}{(K_1 + K_2)(B-1)} \ln|1-\alpha| + \frac{1}{(K_2 B + K_1)(B-1)} \ln|1 - \frac{\alpha}{B}|$$

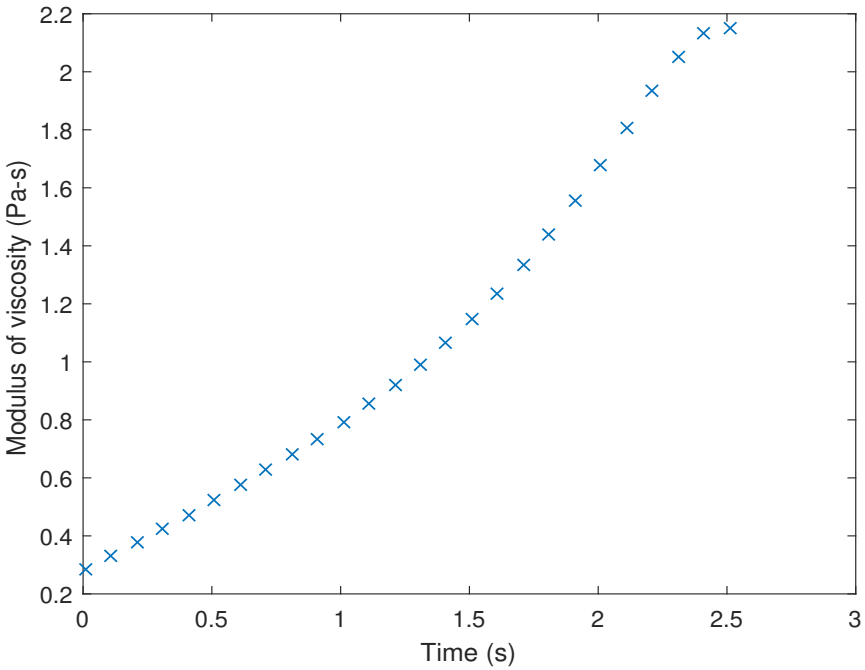

Figure 6.2: Variation of modulus of viscosity with respect to time for 3501-6 resin during curing.

$$+\frac{K_2}{(K_1+K_2)(K_2B+K_1)}\ \ln|1+\frac{K_2\alpha}{K_1}|$$

For $\alpha > 0.3$, we have

$$t = -\frac{1}{K_3}\ln\frac{(1-\alpha)}{0.7} + t_c$$

where,

$$t_c = \frac{-1}{(K_1+K_2)(B-1)}\ln(0.7) + \frac{1}{(K_2B+K_1)(B-1)}\ln|1-\frac{0.3}{B}|$$
$$+\frac{K_2}{(K_1+K_2)(K_2B+K_1)}\ln|1+\frac{0.3K_2}{K_1}|$$

Strain input is considered to be sinusoidal due to the nature of loading for electronic equipments, wherein, $\gamma_0 = 1$ and frequency here is the ul-

trasonic frequency $\omega = 15$khz as the bonding is assumed to be carried out using ultrasonic curing methods that has lower temperature requirement as compared to the traditional curing methods.

$$\gamma_{kl} = \gamma_0 \sin(\omega t) \tag{6.3}$$

The curing temperature considered is 500K for a time period for 2.5 seconds and the variation of degree of cure w.r.t to time as the temperature increases with time is shown in Fig. 6.3.

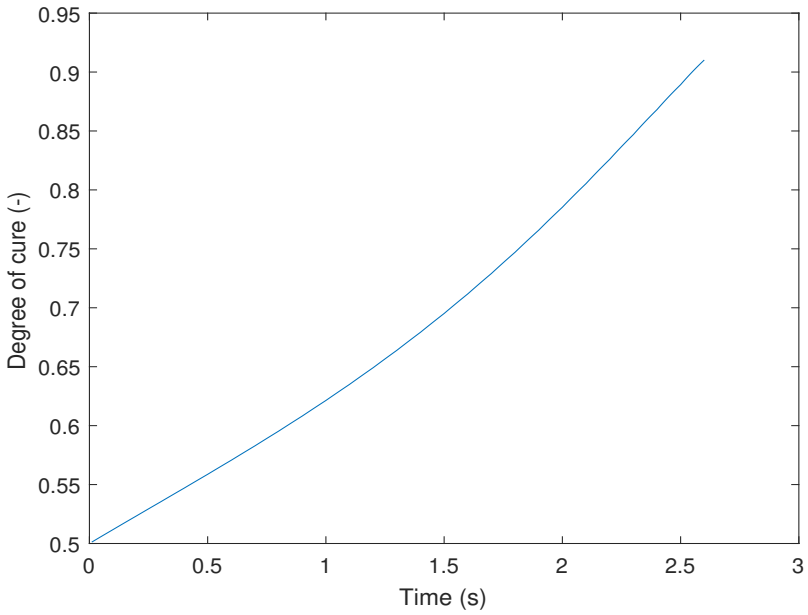

Figure 6.3: Variation of degree of cure vs time as the temperature varies with the progress of cure.

Stress is plotted against time with $dt = 0.0001$ as shown in Fig.6.4. As observed, stress varies in a sinusoidal manner with increasing amplitude which is similar to the trend seen in Fig.**??** for stress variation of

Maxwell model with linearly varying material properties. The higher rate of increase in amplitude for the present case is attributed to the usage of realistic properties i.e. G and η have exponential and power-law distributions, respectively. The rate of increase of these moduli impacts the stress-time characteristics.

$$\tau_{kl}(x,t) = e^{-F(x,t_p)} 2G(x,0)\gamma_{kl}(x,0) \quad + \quad h(t_p)\triangle\gamma_{kl}(t_p) + \quad R_p \qquad (6.4)$$

where

$$R_p = e^{[F(x,t_{p-1})-F(x,t_p)]}\left[h(t_{p-1})\triangle\gamma_{kl}(t_{p-1}) + R_{p-1}\right] \qquad (6.5)$$

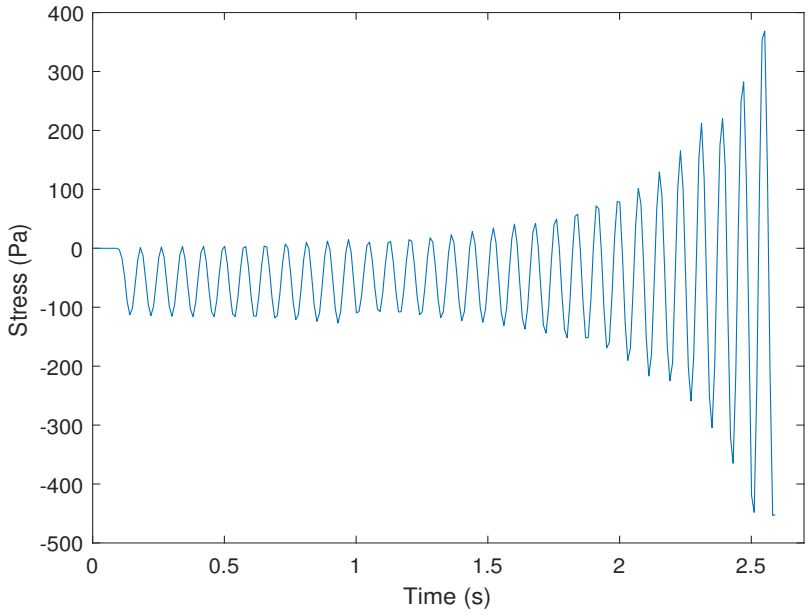

Figure 6.4: Plot of stress vs time using sinusoidal strain input for 3501-6 resin.

Utilizing the calculated stress data, the dissipation energy was determined for small time intervals, and subsequently using Eq.(6.7), the change

in temperature of unit mass of material was calculated. Dissipation energy is given by,

$$W^d = \int_0^{t_p} \frac{[\tau_{kl}(x,t)]^2}{2\eta_1(\alpha)} \tag{6.6}$$

This is equivalent to the amount of heat generated, Q, in Joules defined as

$$Q = mC_p \triangle T \tag{6.7}$$

where m is unit mass in kg, C_p is the specific heat and $\triangle T$ is the change in temperature in K. The specific heat, C_p, is given by Eqs.(6.8) and (6.9). This is obtained from experimental data as For $T < (208.8 + 293.26\alpha_d)$(K),

$$C_p = (-92.7 + 5.347T - 364.2\alpha_d) \tag{6.8}$$

For $T > (208.8 + 293.26\alpha_d)$(K),

$$C_p = (2867.6 - 13.322T + 4.304 \times 10^{-2}T^2 - 3.776 \times 10^{-5}T^3) \tag{6.9}$$

Accordingly, the temperature was updated to the newly calculated value and used to determine material properties and the stress characteristics for the next unit of time. This procedure was repeated until the desired curing time was achieved. As seen in Fig.6.6, a reasonable increase in temperature was observed for the small time period under consideration. It is expected that with additional curing time, a further increase in temperature would be observed.

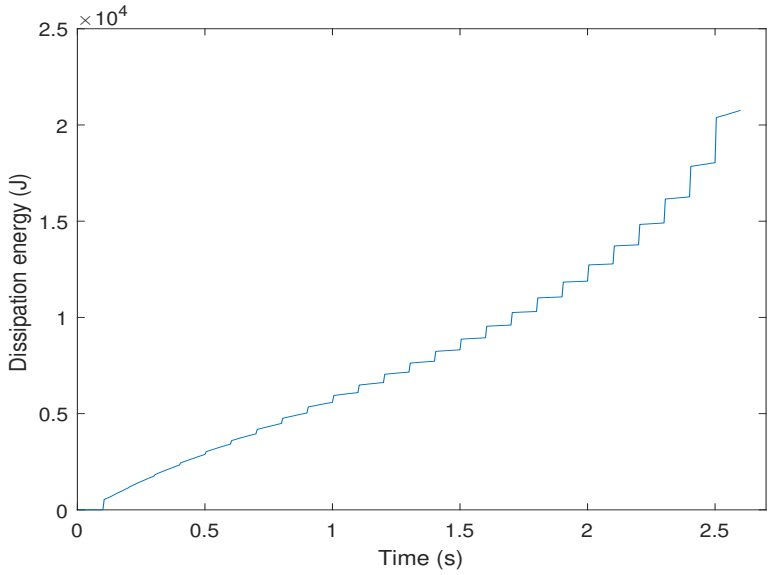

Figure 6.5: Plot of DE vs time for sinusoidal strain input for 3501-6 resin.

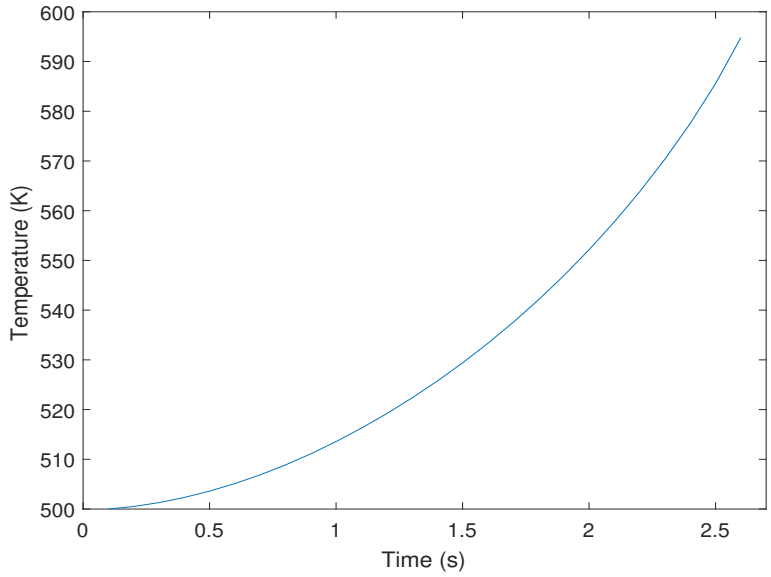

Figure 6.6: Plot of Temperature vs time for sinusoidal strain input using realistic material properties.

7 Conclusions

This study investigated the chemo-thermo cure of viscoelastic polymer materials in order to determine the stress generated and energy dissipated during the curing process. A generalized model that is applicable to any material is essential in order to enable its applicability towards the comparison of different bonding substances, and to optimize curing cycle configurations, and this was one of the fundamental goals of the presently developed numerical model. The mathematical formulation of a viscoelastic material represented by the Maxwell model was implemented using a novel evaluation methodology that helped reduce the computational power requirement by limiting the number of functional evaluations. The commercially-available 3501-6 resin was simulated as a characteristic material on account of its well-studied reaction kinetics and curing characteristics in the literature. The numerical model for Maxwell and Generalized Maxwell models were validated against analytically derived solutions for a constant strain input with constant material properties, and a good agreement was obtained. Simulations were performed for problems with sinusoidally varying strain inputs wherein the materials varied linearly with degree of cure. Lastly, the numerical Maxwell model was used to calculate stresses for 3501-6 resin

wherein, the loading replicated ultrasonic bonding parameters and realistic material properties for $G(\alpha)$ and $\eta(\alpha)$ were chosen (based on experimental data) that varied with degree of cure and temperature.

References

Adolf, D., Martin, J.E., Calculation of stresses in crosslinking polymers, Journal of Composite Materials, 1996, Vol 30, pp. 13-34.

Carlone, P., Aleksendric, D., Cirovic, V., Palazzo, G.S., Meta-modeling of the curing process of thermoset matrix composites by means of a FEMANN approach, Composites: Part B, 2014, Vol. 67, pp. 441-448.

Chern, B.C., Moon, T.J., Howell, J.R., Tan, W., New Experimental Data for Enthalpy of Reaction and Temperature- and Degree-of-Cure-Dependent Specific Heat and Thermal Conductivity of the Hercules 3501-6 Epoxy System, Joural of Composite Materials, 2002, Vol. 36, pp. 2061-2072.

Eom, Y., Boogh, L., Michaud, V., Sunderland, P., Manson, J., Time-cure temperature superposition for the prediction of instantaneous viscoelastic properties during cure, Polymer Engineering and Science, 2000, Vol. 40, pp. 1281-1292.

Hilton, H.H., Yi, S., Analytical formulation of optimum material properties for viscoelastic damping, Smart Materials and Structures,1992, Vol.1, pp.113-122.

Hossain, M., Possart, G., Steinmann, P., A small-strain model to simulate the curing of thermosets, Computational Mechanics, 2009, Vol 43. pp. 769-779.

Hossain, M., Steinmann, P., Degree of cure-dependent modelling for polymer curing processes at small-strain. Part I: consistent reformulation, Computational Mechanics, 2014, Vol. 53, pp. 777-787.

Lee, W.I., Loos, A.C., Springer, G.S., Heat of reaction, degree of cure, and viscosity of Hercules 3501-6 resin, Journal of Composite Materials, 1982, Vol. 16, pp. 510-520.

Liang, G., Chandrashekhara, K., Cure kinetics and rheology of soy-based epoxy resin, Journal of Applied Polymer Science, 2006, Vol. 102, pp. 3168-3180.

Liu, L., Yi, S., Ong, L.S., Chian, K.S., Finite element analysis for microwave cure of underfill in flip chip packaging, Thin Solid Films, 2004, Vols. 462-463, pp. 436-445.

Liu, L., Yi, S., Ong, L.S., Chian, K.S., Osiyemi, S., Lim, S.H., Su, F., Chemothermal Modeling and Finite-Element Analysis for Microwave Cure Process of Underfill in Flip Chip Packaging, IEEE Transactions on Electronics Packaging Manufacturing, 2005, Vol. 28, pp. 355-362.

Liu, Y., Irving, S., Luk, T., Kinzer, D., Trends of power electronic packaging and modeling, 10th IEEE Electronics Packaging Technology Conference, 2008, pp. 1-11.

Loos, A.C., Springer, G.S., Curing of epoxy matrix composites, Journal of Composite Materials, 1983, Vol. 17, pp. 135-169.

Paik, K.W., Yim, M.J., High adhesion triple layered anisotropic conductive adhesive film, US Patent US6878435B2, 2005.

Sadeghinia, M., Jansen, K.M.B., Ernst, L.J., Characterization and modeling the thermos-mechanical cure-dependent properties of epoxy molding compound, International Journal of Adhesion I& Adhesives, 2012a, Vol. 32, pp. 82-88.

Sadeghinia, M., Jansen, K.M.B., Ernst, L.J., Characterization of the viscoelastic properties of an epoxy molding compound during cure, Microelectronics Reliability, 2012b, Vol. 52, pp. 1711-1718.

Saseendran, S., Wysocki, M., Varna, J., Evolution of viscoelastic behavior of a curing LY5052 epoxy resin in the glassy state, Advanced Manufacturing: Polymer I& Composites Science, 2016, Vol. 2, pp. 74-82.

Tu, K.N., Reliability challenges in 3D IC packaging technology, Microelectronics Reliability, 2011, Vol. 51, pp. 517-523.

Tummala, R.R., Sundaram, V., Liu, F., White, G., Bhattacharya, S., Pulugurtha, R.M., Swaminathan, M., Dalmia, S., Laskar, J., Jokerst, N.M., Chow, S.Y., High density packaging in 2010 and beyond, IEEE International Symposium on Electronic Materials and Packaging, 2002, pp. 30-36.

Yang, D.G., Jansen, K.M.B., Ernst, L.J., Zhang, G.Q., Bressers, H.J.L., Jannsen, J.H.J., Effect of filler concentration of rubber shear and bulk modulus of molding compounds, Microelectronics Reliability, 2007, Vol. 47, pp. 233-239.

Yi, S., Hilton, H.H., Constitutive Relations for Thermosetting Resins During Curing Processes, Proceedings of 36th AIAA/ASME/ASCE/AHS/ASC Structures, Structural Dynamics and Materials Conference, 1995, (AIAA-95-1428), New Orleans, Louisiana, USA,. April 10-12.

Yi, S., Hilton, H.H., Ahmad, M.F., A finite element approach for cure simulation of thermosetting matrix composites, Computers and Structures, 1997, Vol.64, pp.383-388.

Yi, S., Liu, L., Sin, C.K., Su, F., Gao, S., A Study of Microwave Curing Process for Underfill used in Flip Chip Packaging. Part2:3D FEM Simulation of Microwave Power Distribution inside Variable Frequency Microwave

Oven, IEEE International Symposium on Electronic Matrials and Packaging, 2001, pp.29 - 33.

Yim, M.J., Paik, K.W., Design and Understanding of Anisotropic Conductive FIlms (ACF's) for LCD packaging, IEEE Transactions on Components, Packaging, and Manufacturing Technology, 1998, Vol.21, pp.226 - 234.

Yim, M.J., Paik, K.W., Recent advances on anisotropic conductive adhesives (ACAs) for flat panel displays and semiconductor packaging applications, International Journal of Adhesion and Adhesives, 2006, Vol. 26, pp. 304-313.

Yim, M.J., Paik, K.W., Preparation method of anisotropic conductive adhesive for flip chip interconnetion on organic substrate, US Patent US6238597B1, 2001.

Zhang, J., Xu, Y.C., Huang, P., Effect of cure cycle on curing process and hardness for epoxy resin, Express Polymer Letters, 2009, Vol 13, pp. 534-541.

Kamal, M.R., Sourour, S., Kinetics and Thermal Charecterization of Thermoset Cure,Polymer and Engineering Science, 1973, Vol 13, pp. 59.